A Low Cost Process for Fabricating FDM Filaments Reinforced with Inorganic Fillers

by

Mohamed Hassanien

A Thesis presented to the Faculty of the
American University of Sharjah
College of Engineering
In Partial Fulfillment
of the Requirements
for the Degree of

Master of Science in
Mechanical Engineering

Sharjah, United Arab Emirates

July 2021

Declaration of Authorship

I declare that this thesis is my own work and, to the best of my knowledge and belief, it does not contain material published or written by a third party, except where permission has been obtained and/or appropriately cited through full and accurate referencing.

Signed *Mohamed Hassanien*

Date: 21/07/2021

Approval Signatures

We, the undersigned, approve the Master's Thesis of Mohamed Hassanien.

Thesis Title: A Low Cost Process for Fabricating FDM Filaments Reinforced with Inorganic Fillers

Date of Defense: 01/07/2021

Name, Title and Affiliation **Signature**

Dr. Maen Alkhader
Associate Professor, Department of Mechanical Engineering
Thesis Advisor

Dr. Bassam Abu-Nabah
Associate Professor, Department of Mechanical Engineering
Thesis Co-Advisor

Dr. Basil Darras
Associate Professor, Department of Mechanical Engineering
Thesis Committee Member

Dr. Mahmoud Awad
Associate Professor, Department of Industrial Engineering
Thesis Committee Member

Dr. Mamoun Abdel-Hafez
Head
Department of Mechanical Engineering

Dr. Lotfi Romdhane
Associate Dean for Graduate Affairs and Research
College of Engineering

Dr. Sameer Al-Asheh
Interim Dean
College of Engineering

Dr. Mohamed El-Tarhuni
Vice Provost for Research and Graduate Studies
Office of Graduate Studies

Acknowledgement

I would like to thank my advisors Dr. Maen Al Khader and Dr. Bassam Abu-Nabah for providing me with everything possible to smoothen the path of this work, being it knowledge or valuable advice.

My appreciation goes to my colleague Omar El Batal for his continuous support whenever I needed help during the experimentation phase.

Not to forget the support and sacrifices that my father, mother and sisters were willing to give. Thank you for everything you have done for me.

I am also grateful for the opportunity I was given by the American University of Sharjah by awarding me with teaching assistantship which served as the foundation of this work.

Dedication

To my father Monir Hassanien, my mother Manal, siblings and friends…

Abstract

Low cost desktop-sized fused deposition modelling (FDM) printers have been widely embraced by small to large scale institutions as well as individuals. Their ease of use and low cost qualified them to become an important enabling platform that enhances creativity and transforms design and modelling processes. To further enhance their utility and add another dimension to the range of possible materials that desktop FDM printers can process, multiple efforts originating from within the desktop FDM community have tried to create low cost desktop sized solutions capable of fabricating customized filaments. These attempts utilized short single screw extruders and did not have the mixing abilities provided by industrial multi-stage twin screw extruders. Therefore, low cost solutions were not effective in fabricating filaments customized with particle based fillers. This work aims to propose a process that enables low cost extruders to fabricate filaments with particle based fillers. In the proposed process, particles are heated and deposited on thermoplastic pellets that are subsequently extruded using a low cost desktop single screw extruder. Depositing the reinforcing particles on the pellets allows for minimizing the need for the mixing process that takes place in industrial extruders. To demonstrate the effectiveness of the process, PLA based filaments with two types of fillers were fabricated from commercial PLA pellets. Fillers used were Dune sand and Silicon Carbide. Dune sand was selected for its availability in the UAE and Silicon Carbide for its high stiffness and strength. Filaments with different particle weight fractions were fabricated and experimentally tested. Filaments' stiffness and strength were measured, and their microstructure along their lateral and longitudinal directions was observed. Improvements in elastic moduli, stiffness and yield strength were recorded for both of the developed reinforced filaments. The effect of aging on tensile strength, elastic moduli and yield strength had been investigated which stems from biodegradability of PLA. Results show that the proposed process can fabricate filaments with multiple types of inorganic fillers. Produced filaments were successfully used to fabricate parts using a commercial Desktop FDM printer.

Keywords: 3D printing, reinforced filaments, filament fabrication, aging.

Table of Contents

List of Figures

Chapter 1. Introduction

This chapter provides an introduction to fused deposition modelling (FDM). In addition, it introduces the problem studied in this work and highlights the contributions of this work to the field of 3D printing. Lastly, it presents a general organization of the thesis.

1.1. Overview

Additive manufacturing has drawn attention due to its advantages over conventional subtractive manufacturing [1]. Additive manufacturing processes fabricate three dimensional parts by joining layers of materials in a computer controlled process. Different joining processes can be used (e.g., sintering, solidification) depending on the particular material and additive manufacturing process used. Advantages inherent to additive manufacturing processes include: reduced material wastage as the constructed part can conform and match the intended design without the need to additional subtractive processes, ability to produce complex geometries that can be impossible or too expensive to make using traditional subtractive processes, eliminating the need for molds and tools which reduces the overhead costs, and can fabricate components using materials that are not easily compatible subtractive manufacturing processes.

The most commonly used additive manufacturing technique is fused deposition modeling (FDM) or fused filament fabrication (FFF) [1]. These are two different names that are used interchangeably to describe the same method. FDM was developed and patented in the late 1980s [2]. In FDM printers, a filament is heated in the printer head and layers from it are deposited on the printing platform. This process is repeated to build the designed part layer by layer from the melting filament, resulting in three dimensional polymeric prototype. 3D printed prototypes helped in visualizing designs, debugging problems and in optimizing solutions. Accordingly, FDM greatly assisted product development cycles across multiple industries. The cost of FDM 3D printers dropped significantly in recent years due to the development of small desktop FDM printers. These provided students, hobbyists and designers with an enabling platform to visualize their designs and increase their creativity. Desktop 3D printers are compatible with few commercially available filaments. The most common are polylactic acid

(PLA), Acrylonitrile Butadiene Styrene (ABS) and Polyvinyl Alcohol (PVA). These thermoplastics can be used for various applications ranging from basic use (PLA and ABS) to advanced engineering and aviation applications (PVA). To increase the utility of 3D printers, there is a need for more types of filaments. More importantly, users of Desktop 3D printers such as scientists, students and designers need to create customized filaments that can provide tailored or enhanced properties such as improved stiffness or strength. Developing customized filaments with improved properties allows for realizing 3D printed parts with enhanced properties. For instance reinforced filaments allow for fabricating intricate structures like cellular solids [3-8] that exhibit increased specific stiffness and strength ratios. On the other hand, developing filaments reinforced with conductive or dielectric reinforcement can aid in fabricating piezoelectric sensors and foams [9-12]. Moreover, customizing filaments using two phase polymers or materials assists in realizing shape memory polymers and 3D printed structures with shape memory ability [13, 14]. Evidently, there is a spectrum of applications that would benefit from developing customized or reinforced filaments. This need motivated the development of desktop based filament extruders. These are low cost solutions that can create filaments from different types of plastics. However, they use single screw extruding mechanism and therefore cannot produce customized filaments comprised from multiple materials. Accordingly, there is a need for a technology or a solution that can allow for creating customized filaments composed of multiple materials. As the audience targeted is users of desktop 3D printers, this technology needs to be cheap and preferably not bigger than desktop 3D printers.

1.2. Problem Statement

Producing 3D printed parts, using FDM, with improved mechanical characteristics requires the development of composite or reinforced filaments. Most of the developed composite filaments are made by modifying existing thermoplastics through the addition of a reinforcing material that could result in an enhancement in the mechanical properties of the overall composite. In most cases, expensive industrial-grade equipment such as twin-screw extruders as well as intricate preparation procedures are required to fabricate composite filaments. So far, users of 3D desktop printers have no cheap option to create their own customized filaments. Low cost extruders available to users of 3D desktop printers utilize single extruding screw; thus,

they do not have the ability to mix multiple phase materials and can only produce single phase filaments. This work attempts to provide users of 3D desktop printers with the ability to create low-cost customized composite filaments. To create the filaments, this work proposes a tailored manufacturing approach that utilizes low cost extruders. In this approach, reinforcing inorganic materials are heated and deposited on plastic pellets. Subsequently, the pellets are fed to a low cost desktop extruder to create customized composite filaments. Depositing the fillers on the pellets minimized the need for mixing and allows low-cost single screw extruders to create composite filaments. This work evaluates the proposed fabrication approach.

1.3. Thesis Objectives

This research will focus on developing a low-cost reinforced filament fabrication process which will enable not only researchers, but also hobbyists to fabricate their own reinforced filaments for various applications. The proposed reinforced filament fabrication process will serve as an easy and cost-effective method that is applicable to many types of thermoplastics and reinforcement, such as particle reinforcement. The need for powdered thermoplastic and reinforcing materials as well as industrial-grade equipment such as twin-screw extruders and pelletizers will be eliminated. The effectiveness of the developed method in terms of reinforcement distribution inside the polymer will be investigated. After that, the influence of adding reinforcing particles to the polymeric material on mechanical characteristics is assessed. Lastly, the printability of the fabricated composite filaments is verified by printing compression samples and evaluating their mechanical performance. The proof of concept of this study considers the fabrication of sand reinforced PLA and Silicon carbide reinforced PLA composite filaments.

1.4. Thesis Organization

The rest of the thesis is organized as follows: Chapter 2 provides background information about FDM, its compatible filaments and works related to this study. The developed method for reinforced filament fabrication process is discussed in Chapter 3. Chapter 4 presents the methods of assessing the mixing method as well as mechanical characterization of the filaments. Chapter 5 discusses the results of this study. Finally, Chapter 6 summarizes the findings of this study and outlines future work.

Chapter 2. Background and Literature Review

2.1. 3D Printing Using FDM Technique

The process of 3D printing begins by feeding a CAD file representing the part to be printed to a slicing software, typically supplied by the 3D printer's manufacturer. Then the part is sliced into a number of layers that form the complete object. Information about these slices are sent from the computer to the 3D printer in the form of G-code commands. A thermoplastic filament is loaded into the printer by feeding the filament into the extrusion head. Once the nozzle reaches the desired printing temperature, which is material dependent, the extrusion head drives the filament into the hot nozzle where it melts. The extrusion head moves in the 3D space above the printing table depositing strands of melted plastic on the printing table according to the G-code delivered to the 3D printer by the printing software. The extrusion head builds the part by depositing layer after layer of the melted filament. All of the layers combined will form the final object as modeled by the designer. 3D printing software, which is the slicing software, allows the user to input and tune the printing parameters such as printing temperature, printing speed, printing orientation, infill pattern, infill density, and bed temperature. Material selection stands as one of the most important decisions a designer would make before printing. There is a wide variety of FDM filaments that are primarily thermoplastics which exhibit different mechanical characteristics.

2.2. FDM Filaments

Thermoplastic filaments look like spools of thick wires, typically 1.75 mm or 2.85 mm (sometimes referred to as 3 mm) in diameter. The most common filaments in the market are made from PLA and ABS. However, for applications that require special mechanical or environmental characteristics, special filaments are available. These are made from PVA, High Density Polyethylene (HDPE), Low Density Polyethylene (LDPE), Polyether Ether Ketone (PEEK) and Nylon 6 (PA 6). The following provides a short description to each one of the aforementioned thermoplastic filaments.

2.2.1. PLA. PLA, also referred to as polylactic acid, is one of the most used thermoplastics to make FDM filaments. PLA, which has chemical composition $(C_3H_4O_2)_n$, is developed from natural resources such as tapioca starch. PLA is environmentally friendly and degrades when disposed in a compostable environment.

Different grades of PLA are available in the market. They align with multiple industrial applications; however, this work considers PLA 4032D which is common in 3D printing applications. A review of PLA properties is provided by Henton, et al. [15].

2.2.2. ABS. Acrylonitril-butadieen-styreen, popular as ABS, is also one of the most widely used polymers in making filaments. ABS, which is known for its shiny and opaque appearance, has higher thermal resistant and tougher than PLA. However, PLA is stiffer and stronger that ABS [16].

2.2.3. Nylon (PA 6). Offers low friction coefficient, high melting point and resistance to abrasion. In addition, it possesses attractive properties such as durability and flexibility [17]. Its properties make it more attractive to engineering applications rather than for just prototyping.

2.2.4. HDPE/LDPE. HDPE (high density polyethylene) provides comparable mechanical properties to those offered by PLA and ABS. However, HDPE may be challenging to deal with in 3D printing due to its crystallization-induced shrinkage during cooling. This phenomenon results in stresses that warp printed parts. LDPE (low density polyethylene) not only suffers from high shrinkage as its HDPE counterpart it delivers lower stiffness and strength. However, HDPE/LDPE are desirable for their recyclability [18].

2.2.5. PEEK. Polyether ether ketone serves as one of the advanced materials in 3D printing industry. PEEK offers relatively high mechanical, thermal and chemical characteristics making it one of the materials considered for critical applications such as aviation [19]. For instance, PEEK has a relatively high temperature resistance as well as elongation. Despite the attractive properties that PEEK offers, there remain some obstacles that hinder its wide spread implementation. For instance, parts printed from PEEK filaments exhibit high dimensional inaccuracy and high surface roughness.

2.2.6. PVA. (Polyvinyl alcohol) is one of 3D printable materials that is desirable for making medications. A study was conducted to validate whether FDM is capable of producing medical caplets that can be consumed through oral administration [20]. PVA was used for this medical application for its ability to dissolute in acidic media.

2.3. Related Work

To obtain 3D printed parts with improved mechanical properties, two routes are followed. The first focuses on the optimization of printing parameters, while the second focuses on the fabrication of reinforced composite filaments that can be used to print 3D components with improves mechanical, thermal and electrical properties. The following provides an insight on both routes with more focus into the second route.

Although PLA has fair mechanical characteristics compared to other polymers, researchers have been trying to improve its characteristics by developing reinforced PLA composites using different types of reinforcing materials. Yu, et al. [21] developed PLA/Talc composite using a nucleating agent. Filament fabrication process started with drying Talc powder in an oven at 103 degrees Celsius for 120 minutes. After that, PLA granules and Talc powder are mixed and melted using a twin-screw extruder. After that, the extruded stranded are pelletized and extruded again in a single-screw extruder. The filaments are then used for the fabrication of testing specimens using FFF process. It was found that PLA/Talc compounds have higher crystallinity. An improvement in crystallinity from 3.6% to 12% was capable of increasing the flexural modulus by 15%. Adding 3% and 6% Talc to a PLA/Talc composite increases the flexural modulus from 3098 MPa (for pure PLA) to 3555 MPa and 3566 MPa, respectively. Increasing Talc percentage in PLA/Talc composites was also observed to result in increased storage modulus [21]. Crystallinity could be also affected by manipulating the cooling rates during the printing process. In the case of neat PLA, higher cooling rates are capable of reducing crystallinity and consequently weaken the mechanical properties (e.g., tensile strength) of printed objects [22]. PLA's mechanical properties were also manipulated through composing PLA/$MgAl_2O_4$:Sm^{3+} Phosphor bioplastic which was developed to obtain a luminescent material. Wire filament fabrication process incorporated the use of twin-screw extruder to melt and mix the powdered material which will be pelletized and extruded using a single screw extruder to form 3D printing filament [23]. The composite bioplastic delivered lower glass transition, crystallization and melting temperatures and higher flexural and tensile strengths as compared to neat PLA. Daver, et al. [24] developed cork-PLA composite with enhanced impact resistance properties. PLA and cork powders are manually mixed and then added to a twin-screw extruder. The produced composite strand is pelletized and extruded into a 3D printing filament

form using a single screw extruder. Testing samples were 3D printed using the produced filaments. It was found that increasing the cork content, as a reinforcing material, in cork-PLA composites decreases the composites' tensile strength and increases its impact strength. The low-density nature of cork has also reduced the density of the overall composite making it score higher specific modulus and tensile strength. To further improve the properties of cork-PLA composites, Tributyl citrate (TBC) was added, resulting in higher ductility and elongation at break. However, printed components from cork-PLA exhibited inferior stiffness and yield strength as compared to compression molded specimens.

To improve the mechanical properties of PLA, Zhou, et al. [25] modified it with butylene adipate-co-terephthalate (PBAT) and carbon nanotubes (CNTs-COOH) with carboxyl groups by using the melt blending technique. To bond the CNTs-COOH nanoparticles with PLA/PBAT matrix, Ethylene-butyl acrylate-glycidyl methacrylate (E-BA-GMA) was used as a compatibilizer that is capable of creating a bond through the interaction between the epoxy and carboxyl groups. The incorporation of CNTs-COOH enhanced the tensile strength, elongation at break, impact strength and thermal stability of PLA. In addition, glass transition, initial degradation temperature and storage modulus increased with the increasing the CNTs-COOH content in the PLA matrix. The optimum dispersion of CNTs-COOH was observed at 0.5 wt% (i.e. weight percent). The optimum dispersion resulted in the best combination of toughness and strength [25].

Reinforcement size and orientation can considerably affect the overall characteristics of reinforced materials or composites. During their study, Lopresti, et al. [26] developed a PLA based reinforced bio-composite that assists in bone tissue regeneration. PLA was used as it has attractive physiochemical properties such as osteo-conductivity. PLA was reinforced using Hydroxyapatite (HA) resulting in PLA-Hydroxyapatite composite. The effect of reinforcement size (nano or micro) and fibres' orientation was further investigated post composite fabrication. The composite showed higher elastic modulus with nano and micro HA; however, nanofibers showed better reinforcement effect. Aligned fibres showed higher elastic modulus compared to randomly aligned fibres. Micro HA increased the brittleness of the composite due to the larger sizes of the reinforcing fibres which acted as local defects in the composite

[26]. Another study was conducted to examine the effect of short carbon fibre content on PLA-carbon fibre composite with varying reinforcement wt% of (0, 3, 5, 7, 10) as well as two bead layup orientation of (0º, 90º) and (-45º, 45º) [27]. It was shown that fracture toughness and fracture energy are higher for CF/PLA compared to neat PLA. Bead layup orientation of 0º and 90º showed higher improvement in fracture energy and fracture toughness compared to -45º and 45º. However, the difference between 0º and 90º, -45º and 45º was minimal hence can be neglected. Higher void content was noticeable with the highest weight percentages of carbon fibre reinforcement (7 wt% and 10 wt%). Effect of nozzle shape on the composite's mechanical characteristics was further investigated by using different nozzle shapes. Square shaped nozzle showed lower inter-bead voids and higher fracture toughness as well as larger bond areas in comparison to circular shaped nozzle [27]. Other printing parameters such as deposited layer thickness are also capable of enhancing neat PLA characteristics. Ayrilmis [28] printed multiple test samples using different deposited layer thicknesses (0.05 mm, 0.1 mm, 0.2 mm and 0.3 mm). Tests showed that increasing the printing layer thickness leads to an increase in the wettability of the printed sample's surface, resulting in higher surface roughness [28]. The effect of infill pattern, layer thickness and printing temperature for PLA/CF composite on tensile strength was investigated by Rao, et al. [29]. It was concluded that the highest tensile strength can be achieved with cubic infill pattern (compared to cubic sub-division and quarter cubic), 0.1 mm layer thickness (compared to 0.2 mm and 0.3 mm) and 225 ºC print temperature (compared to 205 ºC and 215 ºC) [29].

Motivated by developing a composite with improved mechanical characteristics, cheaper value, reduced density, and increased eco-friendliness (biodegradability), Wang, et al. [30] created a micro/nanocellulose-PLA composite. Although the composite achieved improved properties compared to neat PLA, melt flow drastically decreased which required the addition of silane coupling agent (KH-550) to compensate for the drop in melt flow. In addition, the process of preparing the micro/nanocellulose was fairly complex [30].

Material anisotropy of 3D printed components is one of the most important factors that need to be considered while developing composites with improved properties. Fayazbakhsh, et al. [31] investigated the anisotropy of mechanical

characteristics such as tensile strength, modulus, and failure strain as well as gap (also referred to missing extrudent) distribution in 3D printed samples. Strength, modulus and failure strain were found to be higher along the printing direction. Gaps perpendicular to loading direction resulted in weaker mechanical properties along the transverse direction [31].

To improve the mechanical properties of ABS, it was reinforced by TLCP (Thermotropic Liquid Crystalline Polymers) [32]. The reinforced ABS exhibited a relatively high tensile strength and modulus as the reinforcement is nearly continuous. The printing phase was operated at an adequate temperature for melting ABS, not TLCP which has higher melting temperature. The composite exhibited different material properties depending on the shaping technique. The printed material scored a slightly lower tensile strength and modulus compared to compression moulded specimens. Due to the difference in the melting temperature of TLCP and ABS, a dual screw extruder was used to fabricate the composite filaments. Print orientation significantly affected the tensile strength and tensile modulus of the composite. 0º print orientation delivered the highest tensile properties compared to -45º/45º and 90º [32]. Motivated by improving the Young's modulus, ABS reinforced with Polycarbonate (PC) and Graphene pellets (nanofiller) was developed. The composite exhibited significantly increased Young's modulus and glass transition temperature [33]. ABS was also reinforced with carbon nanotubes to improve its mechanical properties. ABS-MWCNT (Multi Wall Carbon Nanotubes) composite was developed and analysed using different weight percentages of MWCNT [34]. ABS granules and MWCNT powder were mixed and put in a twin-screw micro-compounder. After that, the produced element is put into a single-screw extruder to prepare filament compatible with 3D printers. Results showed that the mechanical properties improved considerably with the increase of MWCNT content; however, the brittleness (from ductile to brittle) increased as well. The electrical properties such as conductivity of the composite improved with the presence of MWCNT. Effect of printing parameters such as raster angle on the mechanical properties was further looked into. The raster angle has a substantial influence on the mechanical properties of the composite. Raster angles of 0º and 90º resulted in higher mechanical properties compared to -45º and 45º. To properly disperse the MWCNT reinforcement in the composite, a micro-compounding extrusion machine was used.

ABS reinforced with long carbon fibers was proposed for improved mechanical properties [35]. The composite was called LFT (Long Fiber Thermoplastic) pellets. To fabricate parts from this composite, LFT pellets were first produced. Pellets were injected into moulds to create parts or converted into filaments using twin-screw extruders. Filaments were used to create parts either through 3D printing or injection molding. The pellets were made of different lengths. Pellets made using LFT exhibited higher aspect ratio compared to neat ABS, resulting in enhanced mechanical, thermal, and impact properties. The increase in pellet size significantly enhanced the properties. It is mention-worthy that long fibres required a special extrusion machine which draws the long fiber into an impregnation die to fabricate the filament. Successful enhancement in the thermo-mechanical properties of ABS was also realized by enforcing ABS with Iron and Copper [36]. ABS pellets were produced by pelletizing ABS filament using a mechanical chopper. The pellets are then ground to a particle size of approximately 500 μm using cryogenic grinding technique. Ground ABS and metallic particles are loaded in a multi-variable speed homogenizer. Surfactant is added to improve the dispersion of metal particles in the polymer. 3D printing filament is then produced by loading the composite mixture in a single-screw extruder. After that, iron reinforced ABS and copper reinforced ABS filaments were analysed using dynamic mechanical analysis techniques. Thermal and mechanical properties were considerably improved with the incorporation of metallic particles. Increasing the particles' content increased the thermal conductivity and decreased the heat capacity of the ABS reinforced composite. However, tensile strength of Iron reinforced ABS was observed to be lower than that of virgin ABS. This was related the morphology of the oxide on the surface of the metallic particles as well as the environmental stability of the oxide films.

Few efforts were exerted to develop thermoelectric filaments. ABS-Bi_2Te_3 mixture was used as a thermoelectric filament for forming intricate geometries through FFF processes [37]. The material was mixed in powder-like form, extruded, printed, sintered and characterized. The electrical properties such as conductivity and Seebeck coefficient were improved with high sintering temperatures. FFF delivered a merit figure of 0.54 which is five times higher than that of SLS. In addition, lower porosity as well as low contamination and oxidization levels contributed to the enhancement of the electrical properties. Another interesting mixture was ABS $BaTiO_3$ which was

produced in filament form and printed in several geometrical shapes to confirm its usability as a dielectric material. The results showed that this material, being fabricated using FDM technique, can be a viable option for producing intricate shapes using dielectric materials [38]. Isakov, et al. [39] investigated mixing inorganic ceramic-powder polymer (high permittivity) to ABS (low permittivity). This was motivated by developing dielectric materials that can be used for producing metamaterials with electromagnetic properties and tuneable operational frequencies. However, the process of adding inorganic ceramic-powder polymer to ABS is fairly complex and requires additional machining processes (such as milling) followed by extrusion [39].

Multiple studies were conducted to enhance the properties of Nylon used in 3D printing. An over view of these studies is provided in this section. Using Al_2O_3 to reinforce Nylon-6 resulted in improved overall mechanical performance [40]. The effect of single particle size (SPS), double particle size (DPS) and triple particle size (TPS) of Al_2O_3 reinforcement on the mechanical properties of Nylon 6 composites have been studied [40]. Mechanical properties studies included yield strength, tensile strength, and Young's modulus, to name a few. SPS resulted in the highest percentage elongation, while DPS resulted in the highest yield strength, tensile strength and Young's modulus. Filling pattern, fibre orientation, as well as filling percentage in neat Nylon and reinforced Nylon (i.e. reinforced with fibre glass, Kevlar, and carbon fibre) were investigated [41]. The proposed reinforcement types were divided into two categories: isotropic layers of fibres and concentric rings of continuous fibres. It was shown that the optimal filling pattern without reinforcement was triangular with a filling percentage of 20%. The optimal fiber orientation was 0º compared to 45º and 60º. Best fatigue response was exhibited by carbon fiber reinforced nylon aligned at 0º rather than Kevlar and fiberglass reinforcements. Concentric rings of fiber reinforcement were also studied. The configuration of two rings and 4 layers achieved better fatigue response compared to 4 rings and two layers. Tan and Low [42] fabricated a conductive filament made of HDPE/Nylon-6. Nickel and Tin alloy particles were added to the mix to increase the conductivity of HDPE/Nylon-6. The particles were mixed to a melt that subsequently was extruded using a single screw extruder. The conductivity was increased from a 1,000 S/m to 31,000 S/m with 30 vol% metal loading. Thermal conductivity as a function of whisker amount for HDPE/PA6/alumina composite was studied by García-Fonte, et al. [43]. It was found that thermal

conductivity increases with the increase in whisker amount; however, the maximum values were observed at 50/50 HDPE. This is due to that PE has a higher effective filler amount than other polymers [43].

Schirmeister, et al. [44] addressed many of the issues faced while printing with HDPE such as shrinkage, voiding, warpage, and poor adhesion. Furthermore, Schirmeister, et al. [44] realized improved Young's modulus, tensile strength and surface quality that were comparable to the values obtained by injection molding. The improved properties were achieved by varying the printing parameters such as nozzle diameter, temperature, extrusion rate, build plate temperature and build plate material. The results of the study showed that print speed and nozzle diameter impair surface quality only, leaving mechanical properties unaltered. Extrusion rate gradients; however, prevent void formation. A temperature of 220 ºC and nozzle diameter of 0.8 mm or 240 ºC for a nozzle diameter of 0.4 mm were the best combinations for improving the mechanical properties and minimizing anisotropy. The poly styrene-block-ethene-co-butene-block-styrene (SEBS) build plate material proved to be the best for after processing work (efficient adhesion), where the printed object can be detached by bending the base plate without causing any damages to the built part compared to glass/roughened HDPE and other materials. Dependence of melt strength and drawability of LDPE, HDPE and HDPE/LDPE blend on extrusion temperature and extrusion rate was investigated by Liang [45]. LDPE, HDPE and HDPE/LDPE blend showed lower melt strength at higher extrusion temperatures and increased melt strength at higher extrusion rates. Drawability was improved by increasing the extrusion temperature and reducing the extrusion ratio. This ratio is defined as ratio between the initial cross-sectional area of the part divided by the final cross-sectional area of that part [45]. Fly ash reinforced HDPE was developed to produce a 3D printing filament that can be produce closed cell foams [46]. The effect of adding cenosphere fly ash (environmentally pollutant) to HDPE material was analysed. The addition of fly ash cenospheres reduced the density of the filament making it light-weight. In addition, adding fly ash particles increased the tensile, storage and loss moduli of fly ash reinforced HDPE. On the other hand, melt flow index as well as strength of the filament were reduced with the addition of cenosphere fly ash. In addition, the filament exhibited higher crystallization temperature and lower crystallinity percentage with the increase in fly ash cenospheres content [46]. Cardboard dust reinforced HDPE filament was

fabricated with varying weight percentage (20%, 50%, 75%) of cardboard dust [47]. The fabrication of the filament was successful; however, the properties of the filament were undesirable. Elastic moduli, toughness, stiffness and strain at break decreased with the increasing the reinforcement content. Further, the filament gained a larger diameter and lower density with the increase in cardboard dust content.

Motivated by enhancing 3D parts printed using PEEK filaments, both PEEK filaments' constituents as well as printing process parameters were investigated [48]. Printing and extrusion speeds were observed to affect the microstructure of PEEK filament as well as printed parts' dimensions. In addition, high melt pressure during PEEK filament extrusion was observed to correlate with enhanced filament surface morphology and reduced probability of defects. Optimized control algorithm of speed that mathematically replaces the diameter of the nozzle by the diameter of the filament produced better surface quality, improved dimensional accuracy and better stability. High viscosity of melt PEEK is classified as one of major hurdles that complicated 3D printing using PEEK filaments. To solve this issue, adding IF-WS_2 nanoparticles was proposed [49]. Adding these particles reduced the melt viscosity by 25%. Moreover, adding IF-WS_2 nanoparticles (2 wt%) to PEEK resulted in increased crystallization, storage modulus and degradation temperature. Thus, IF-WS_2 nanoparticles act simultaneously as a lubricating and reinforcing agent. The interlayer adhesion in 3D printed PEEK was investigated by Basgul, et al. [50]. In this study, annealing was used to remove undesired porosities. However, results showed that annealing had almost no effect on removing undesired porosities. In addition, the mechanical properties were not affected by annealing except at lower printing speeds, where some improvement in the mechanical properties were observed. Other attempts to improve PEEK properties tried creating textile composites made of PEEK and coated with silver [51]. Each coated textile fiber serves as a conductive filament. The composite showed favourable electromechanical properties that are desirable for biomedical applications such as strain sensors. Such conductive filaments can potentially be utilized to 3D print cellular-based metamaterials with tailored acoustic properties (e.g. [52-58]). To improve the structural properties of PEEK filaments, they were reinforced with carbon nanotubes (CNT) [59]. CNT PEEK filaments were manufactured using a twin-screw extruder. After testing, it was found that adding CNT to PEEK did not affect the mechanical properties of PEEK; it only made it more brittle. The effect of printing parameters on

the mechanical characteristics of parts 3D printed from PEEK filaments was conducted to find the optimum printing parameters [60]. Results suggested that using a temperature of 440 ºC, a printing speed of 20 mm/s and a layer thickness of 0.1 mm allow for achieving reduced surface roughness and internal defects as well as strong binding between the deposited layers.

Few efforts explored the sustainability dimension of 3D printing. These focused on biodegradable materials such as LDPE and PET [61]. In addition, they used natural additives such as cotton, jute, flax and coir as reinforcements [62]. Results showed that natural additives can improve the mechanical properties of biodegradable filaments. They can increase filament's stiffness, tensile strength and ductility.

The aforementioned review shows that numerous studies aiming to enhance the mechanical, thermal and electrical performance of 3D printed thermoplastic parts were conducted. Improving the characteristics of FDM compatible thermoplastic materials would widen the area of applications of FDM. Previous efforts achieved promising results by reinforcing thermoplastic materials with different types of reinforcing fillers. However, reinforced filaments were fabricated using intricate processes that require expensive industrial-grade equipment such as twin-screw extruders and shear mixers. However, to provide the ability of creating customized filaments to a wider range of audience, there is a need for developing a simple and cost-effective process that can be adopted easily, in particular by the community using FDM. This study offers a simple low-cost method that enables FDM users, particularly users of desktop sized printers, to manufacture reinforced filaments using cheap single-screw extruders. The process and its range of applicability are discussed in details in the following chapters.

Chapter 3. Methodology

3.1. Mixing Polymeric Pellets with Reinforcing Particles

This study considers PLA 4032D for the desirable environmentally-friendly characteristic it possesses, that is, biodegradability [63]. The reinforcing particles are chosen to be dune sand as well as 40 µm Silicon Carbide (SiC). Dune sand was selected for its abundance and low-cost compared to other types of fillers. It was sourced from United Arab Emirates desert which mainly consists of silicates such as silicon-dioxide (SiO_2), in addition to carbonates and quartz [64]. To remove larger sand particles, sand was sieved using a 250 µm mesh screen. SiC particulate reinforcement was chosen for its attractive mechanical properties (i.e. high stiffness and strength). 40 µm SiC particles were supplied by McMaster-CARR, United States of America. Mixing reinforcing particles with the polymeric material is the most important stage of reinforced filaments fabrication. The process begins with weighing PLA pellets that are typically 2-3 mm in size using an electronic scale. The desired weight percentage of particle reinforcement is measured using the same electronic weight scale. To satisfy the low-cost object of this work, a desktop single-screw filament extruder is used. Single-screw extruders cannot mix multiphase micro-particles. Accordingly, they cannot readily create filaments from polymeric pellets and sand or SiC particles. To overcome this issue, the reinforcing particles need to stick to the pellets before their addition to the extruder. To stick the reinforcing particles to the PLA pellets, the reinforcing particles were placed in an electrical oven and their temperature was raised to 300 ºC to ensure that the particles will remain at a temperature higher than the melting point of PLA when they are taken out of the oven and manually mixed with PLA pellets. After the reinforcing particles reached the set temperature, the particles were deposited on the PLA pellets. This process was performed manually. Reinforcing particles were gradually poured and manually mixed with the polymeric pellets which were kept at room temperature. During this process, the hot reinforcing particles adhere to pellets due to localized melting. Manual mixing was continued until all added particles adhered to the pellets, forming composite pellets. Mixing speed is a process parameter to be further investigated in a future study. To ensure that the desired weight percentage of reinforcement is reached, the composite material was weighed again. Besides pure PLA, seven different weight percentages of PLA-sand filaments were developed,

namely, 0.5 wt%, 2 wt%, 3 wt%, 4 wt%, 10 wt% and 15 wt% sand in PLA. However, PLA-SiC filaments were fabricated with 0.5 wt%, 1 wt%, 1.5 wt%, and 2 wt% of SiC reinforcement. Figure 3.1 shows PLA pellets covered in sand particles that were prepared for extrusion process. Higher quantity of sand particles covers larger surface area of individual PLA pellets which makes it look darker in colour.

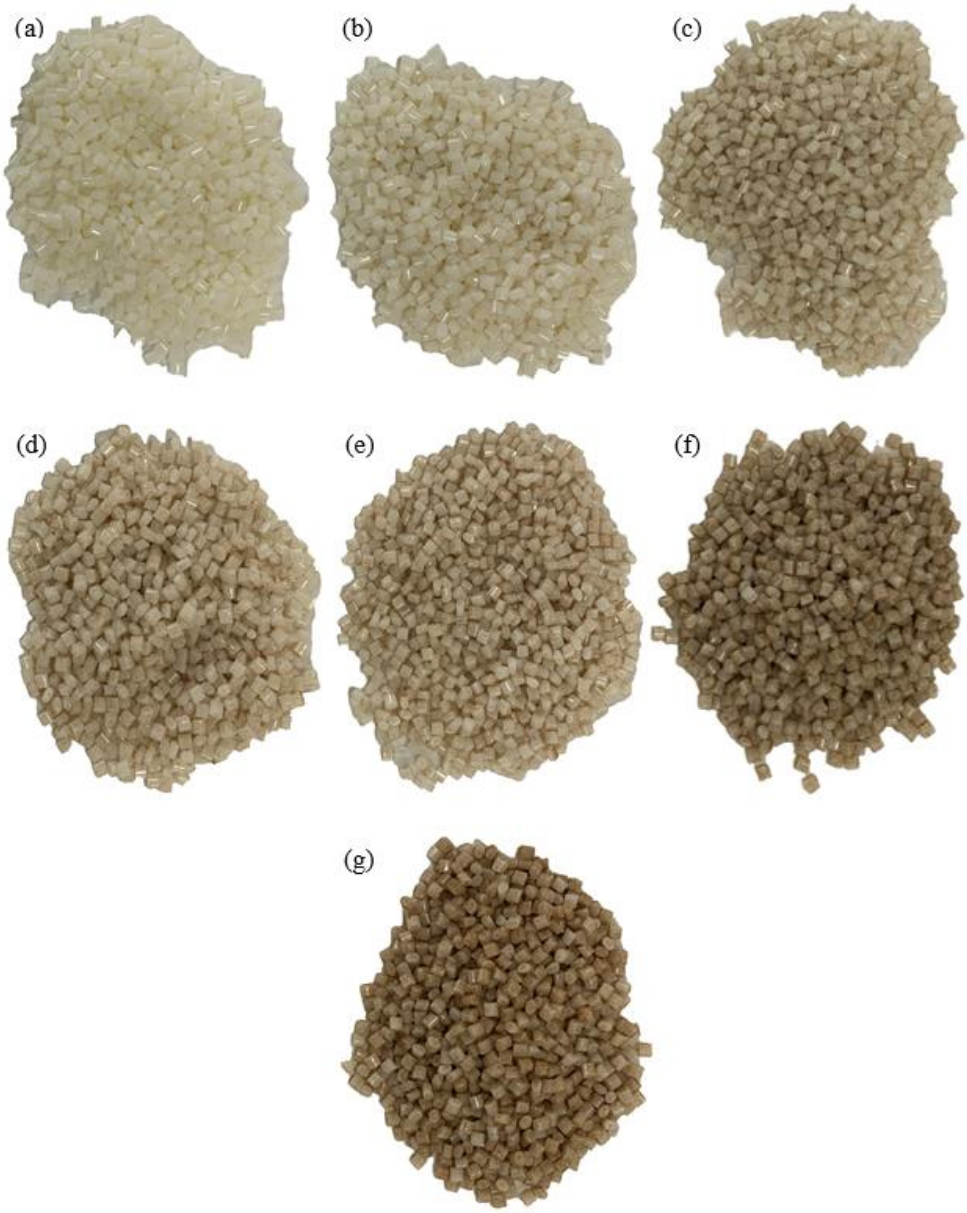

Figure 3.1: PLA pellets covered in (a) 0 wt%, (b) 0.5 wt%, (c) 2 wt%, (d) 3 wt%, (e) 4 wt%, (f) 10 wt%, and (g) 15 wt% sand.

SiC reinforcement is chosen as the second type of reinforcing material for its favourable mechanical characteristics such as high elastic modulus and strength. The same procedure is followed with SiC particles; however, due to significantly higher

thermal conductivity of SiC which can reach up to 120 W/m.K as well as smaller particle size of SiC compared to sand, the mixing phase was done by pouring and mixing the hot particles with pellets directly after taking the particles out of the oven. SiC particles could lose significant amount of thermal energy due to natural convection in a matter of seconds. In case of poor adhesion between the polymer and reinforcing particles due to loss in thermal energy, the remaining particles are retrieved by sieving and weighing the particles that did not adhere to the pellets. Once that is done, the loose particles undergo heating and the mixing process is repeated. This process is repeated until the desired weight percentage of reinforcement is achieved. Four batches of PLA-SiC composite are shown in Figure 3.2. Surface area of individual PLA pellets seem to be entirely covered with SiC particles at 2 wt%. After the preparation of composite pellets, it is important to take it directly to the next step due to the hydrogenic nature of PLA. In case of any delay, it is important to store the pellets at low humidity levels. Figure 3.3 shows microscopic images of individual PLA pellets covered with reinforcing particles.

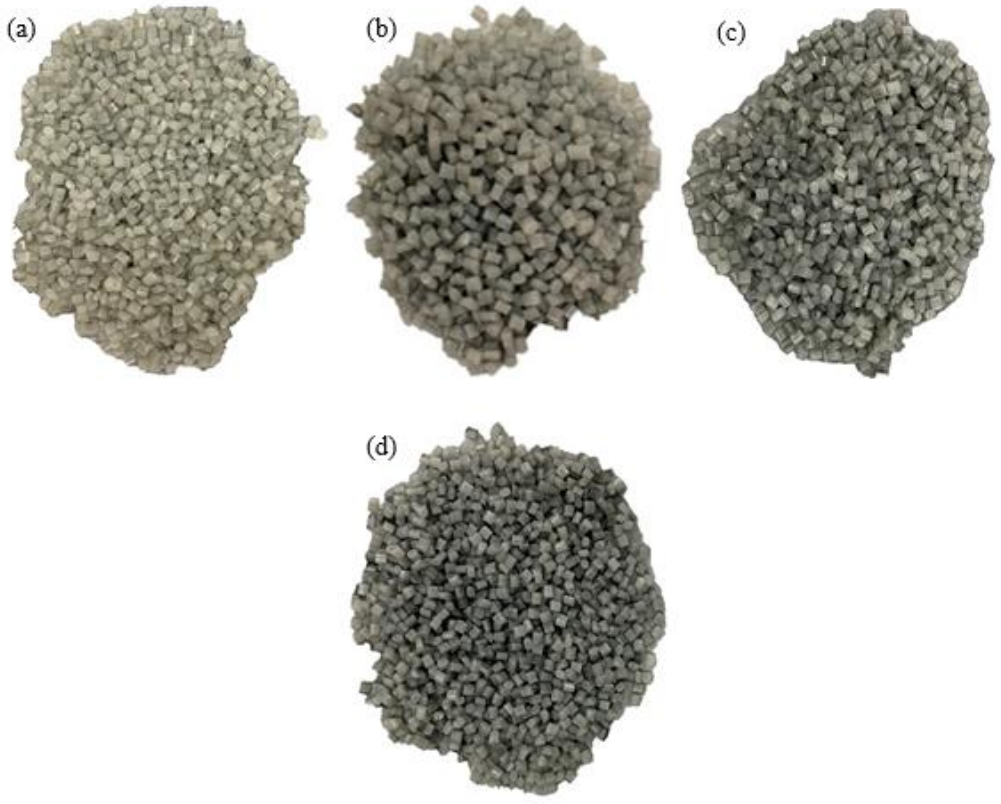

Figure 3.2: PLA pellets covered in (a) 0.5 wt%, (b) 1 wt%, (c) 1.5 wt%, and (d) 2 wt% SiC.

Figure 3.3 shows neat PLA, 2 wt% PLA-sand and 2 wt% PLA-SiC pellets. Sand particles can be distinguished by their dark color (black spots) while SiC particles are the dark (as well as shiny) spots on the surface of PLA pellet. A wider scatter of particles is observed in SiC covered PLA pellet than sand covered PLA pellet. This is due to the relatively smaller particle size of SiC compared to the size of sand particles.

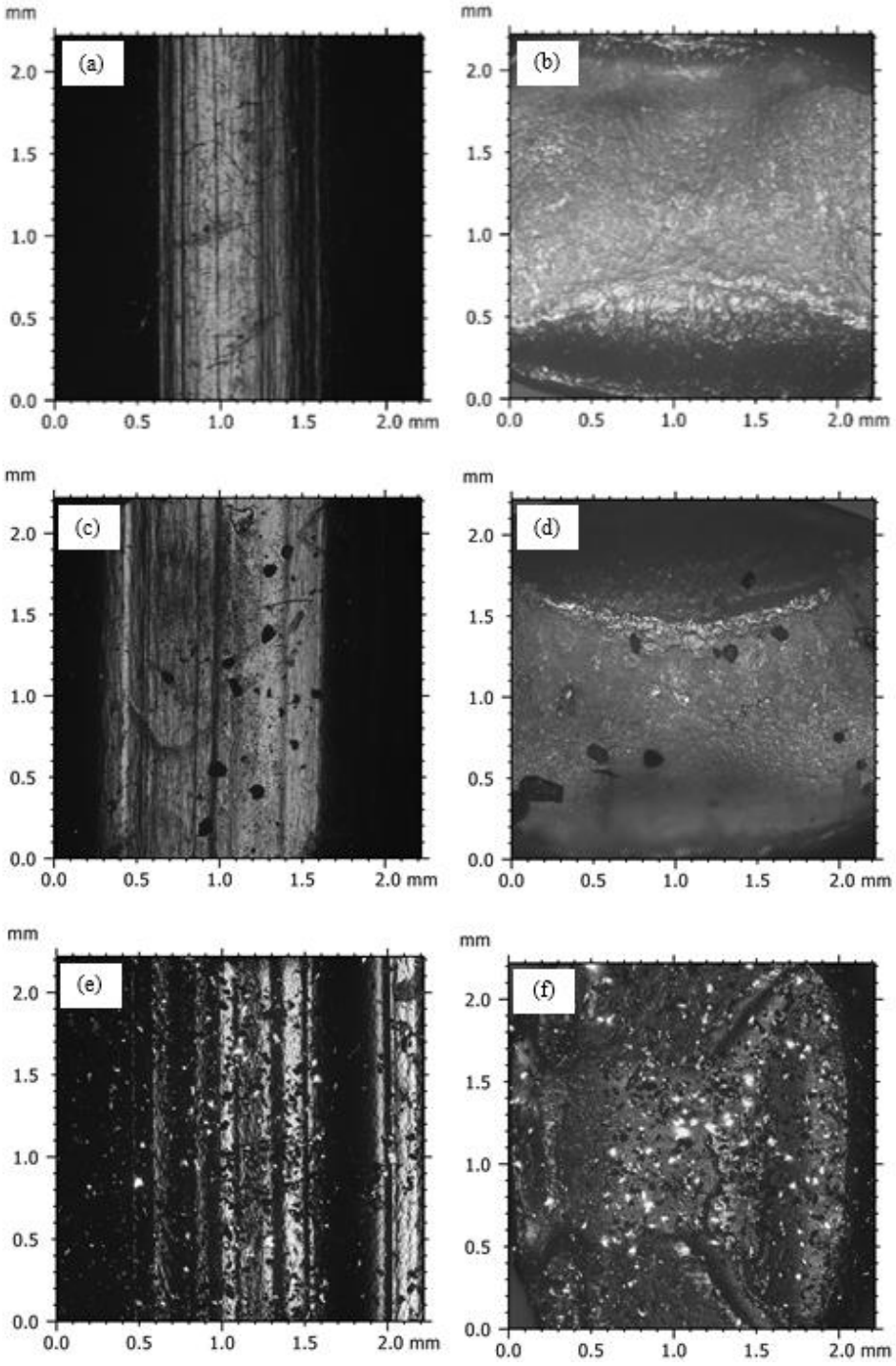

Figure 3.3: Microscopic images of individual pellets for side view and top view of (a)~(b) neat PLA, (c)~(d) PLA-sand, and (e)~(f) PLA-SiC, respectively.

3.2. Filament Extrusion

After the preparation of composite pellets, the next step is to shape the pellets in the form of 1.75 mm filaments compatible with FDM 3D printers. Well Zoom Type B single-screw extruder was used for this purpose. Extrusion temperature is set to 190 ^{o}C which is slightly above the melting point indicated by the manufacturer of PLA pellets to ensure proper melting of the polymeric material. The extrusion speed is fixed at 650 mm/min, which is the machine's highest extrusion speed. High extrusion speed will result in high build up pressure at the extrusion head which will reduce diameter variation of the produced filament. Each batch has 25 grams of pellets to produce approximately 3 meters of filament. The extruder must be flushed with at least 10 grams of neat PLA pellets to remove any residues from the preceding extrusion. Prepared filaments are directly taken for printing and/or testing to avoid excessive exposure to humidity which accelerates the biodegradation process of PLA and therefore alters filaments' mechanical properties. Figure 3.4 shows samples of the fabricated PLA-sand filaments. Darker shades of brown colour are noticed as sand weight percentage increases which primarily comes from the colour of sand particles.

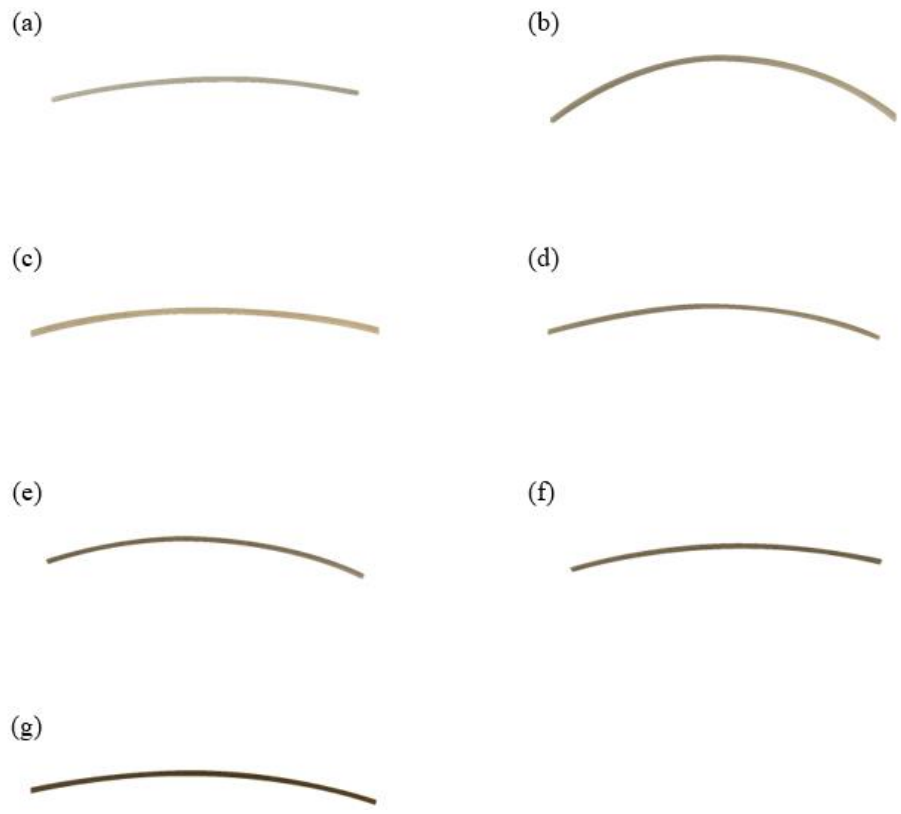

Figure 3.4: PLA-sand filaments with (a) 0 wt%, (b) 0.5 wt%, (c) 2 wt%, (d) 3 wt%, (e) 4 wt%, (f) 10 wt% and (g) 15 wt% sand.

The extruding machine was flushed and purged after the PLA-sand filaments were extruded. Subsequently, PLA-SiC filaments were fabricated. The extruder was flushed avoid any contaminants in the filament that would induce errors in our study. Figure 3.5 shows samples of PLA-SiC filaments that were fabricated with four different weight percentages of SiC in PLA, namely 0.5 wt%, 1 wt%, 1.5 wt% and 2 wt%. Since the colour of SiC particles is dark grey, SiC reinforced filaments have different shades of the same colour depending on reinforcement content.

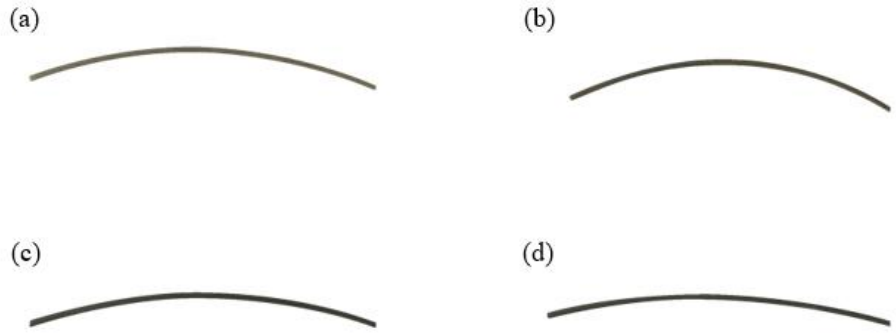

Figure 3.5: PLA-SiC filaments with (a) 0.5 wt%, (b) 1 wt%, (c) 1.5 wt% and (d) 2 wt% SiC.

Chapter 4. Experimental Setup

4.1. Microscopy

To validate the developed mixing method, samples of the fabricated composite filaments were studied under the microscope. Cross-sectional and longitudinal samples were mounted using ClaroCit cold molding kit. As recommended by the manufacturer Struers, ClaroCit powder and ClaroCit liquid are mixed in the ratio of 5:2 by volume. Five specimens of a given reinforcement weight percentage for each composite filament were used in one mounting. The mould is left to cure for at least 20 minutes at room temperature. To look at the distribution of reinforcement inside the polymer, removal of several layers of material in both cross-sectional and longitudinal samples is required. The moulds underwent several dry and wet sanding levels using metallography grinding and polishing machine. Starting with dry roughing stage, the grinding wheel is equipped with P80 SiC paper and set to 150 rpm. After the removal of approximately 0.5 mm of the material, P240 SiC paper is used. During the use of P240 paper, it is recommended to switch back and forth between dry and wet sanding. When reduction in scratch depth is visually noticed, P240 paper is replaced with P800 SiC paper. After reaching to P800, complete switching to wet sanding along with gradual adjustment of the speed to 300 rpm is performed. The last two stages of wet sanding used P1200 and P2500 papers and produced a relatively smooth surface. To further reduce the effect of sanding process on the surface finish of the samples, polishing process was carried out. With grinding wheel set to 200 rpm, velvet polishing cloth is used with Struers polishing compound. Microscope images were taken for each weight percentage of reinforcement in PLA-sand and PLA-SiC specimens using Zeiss Smartproof 5 microscope.

4.2. Tension and Compression Testing

To assess the mechanical performance of the developed composite filaments, their stress-strain behaviour is measured using an Instron Universal Testing Machine (UTM). The machine is equipped with 100 kN load cell, which is adequate for the purpose of this study.

4.2.1. Tensile testing. Since the tensile grips may result in stress concentration on the polymeric filaments, custom grips were designed and manufactured. The

aluminium grips are designed to have the dimensions of 20 x 20 x 4 mm with 2 mm groove in the middle. Each sample requires two grips. The grips are as shown in Figure 4.1. Before placing the filament in the grips, super glue is used to stick the filament to the grips to avoid any slippage during testing. The overall and gauge length of each sample was 100 and 60 mm, respectively. Rate of displacement was fixed at 2 mm/min to maintain a constant strain rate of 5.6×10^{-4} s^{-1} for all samples. For each composite filament, at least four samples were tested. To avoid errors due to variation in the diameter of the filaments, the average diameter was recorded at five different locations on each testing sample.

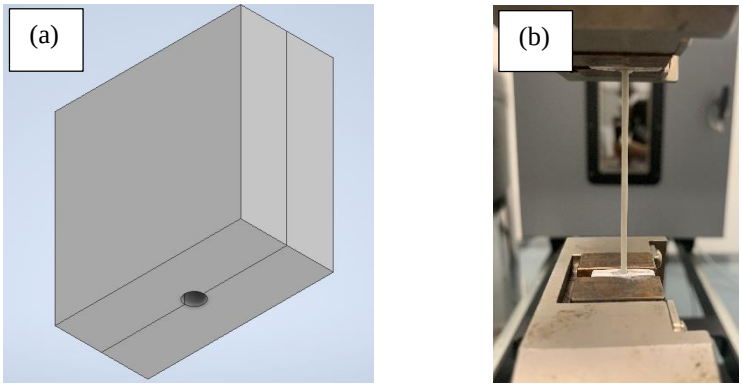

Figure 4.1: (a) Design of filament grip for tensile testing and (b) tensile testing setup.

The mathematical relations that are used to calculate the engineering stress σ and engineering strain ε are given by the equations (1) and (2) where F is the applied force, ΔL is change in length due to deformation, and L is the gauge length of the specimen. The cross-sectional area A is calculated using equation (3).

$$\sigma = \frac{F}{A} \tag{1}$$

$$\varepsilon = \frac{\Delta L}{L} \tag{2}$$

$$A = \pi r^2 \tag{3}$$

After several tensile tests on both sand and SiC reinforced filaments, it was observed that: the filaments do not undergo necking before failure and they fail at small loading force (less than 5% of the machines capacity). Accordingly, the compliance of the machine was ignored and the engineering strain was computed using the cross-head's displacement reported by the machine.

4.2.2. Compression testing. Since it is difficult to test filaments under compressive loading, 10 x 10 x 10 mm samples were printed from the sand and SiC reinforced filaments using a LulzBot Taz 6 3D printer. Due to dimensional variation across the 3D printed specimens, the displacement rate was adjusted for each sample to maintain a strain rate of $5.6x10^{-4}\,s^{-1}$. At least three samples were printed and tested from each of the developed filaments. In some cases, it was decided to reduce the number of testing specimens from five to three due to the significant amount of material each sample requires for printing. Each sample needs approximately 60 cm of filament and a printing time of 45 minutes. For engineering stress calculations, the diameter was recorded as the average of four readings. Engineering stress, engineering strain as well as the area were calculated based on the equations (1)~(3).

(a) (b)

Figure 4.2: 3D printed PLA-SiC compression sample (a) side-view and (b) top-view.

4.3. 3D Printing

Cylindrical samples of 10 mm height and 10 mm diameter were 3D printed using for compression testing. Printing parameters were fixed for PLA-sand as well as PLA-SiC filaments. Printing temperature and speed were fixed at 200 ºC and 15 mm/s. Layer thickness was 0.05 mm whereas the infill density was set to 100%. Bed temperature was set to 60 ºC to make the first layer of the print adhere to the printing table. To further improve the adhesion between the printed part and printing table, hair spray was applied to the printing table 5 seconds before the printing process begins. Since hair sprays are typically volatile, it will assist the first layer of the print to stick to the printing table without affecting the printed part itself. To increase the stability of the part during printing, a brim support was chosen as shown in Figure 3.6 (a). In some cases, the print quality was compromised and sharp edges appeared in the printed cylinder. Therefore, sanding was occasionally required to smoothen the edges of the 3D printed compression samples as shown in Figure 3.6. After multiple prints, the printer's nozzle required clean-up as the abrasive particles in the filaments managed to stick to it. This issue could be resolved by using a harder nozzle such as steel nozzles. Figure 3.6 (a) shows a set of five compression samples that were printed at once using

2 wt% PLA-SiC filament. The extra material shown on the edges of the compression samples can be removed by careful sanding of each compression sample. Figure 3.6 (b) shows the same five samples after sanding.

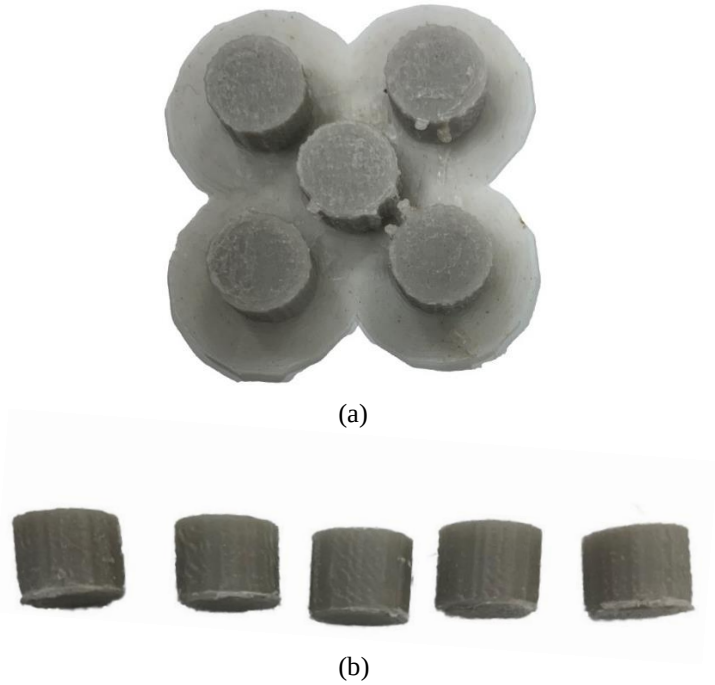

(a)

(b)

Figure 4.3: 3D printed compression specimens made of PLA-SiC composite (a) after completion of printing and (b) after sanding.

Chapter 5. Results and Analysis

5.1. Reinforcement Distribution

To distinguish reinforcement particles from voids in the material, the reinforcing particles were studied separately to estimate their particles size as shown in Figure 5.1. The particle size was recorded by averaging the size of ten samples. Average particle size for dune sand was found to be 150 µm. Although SiC particles were labelled to have 40 µm average particle size, the measured average particle size was 53 µm.

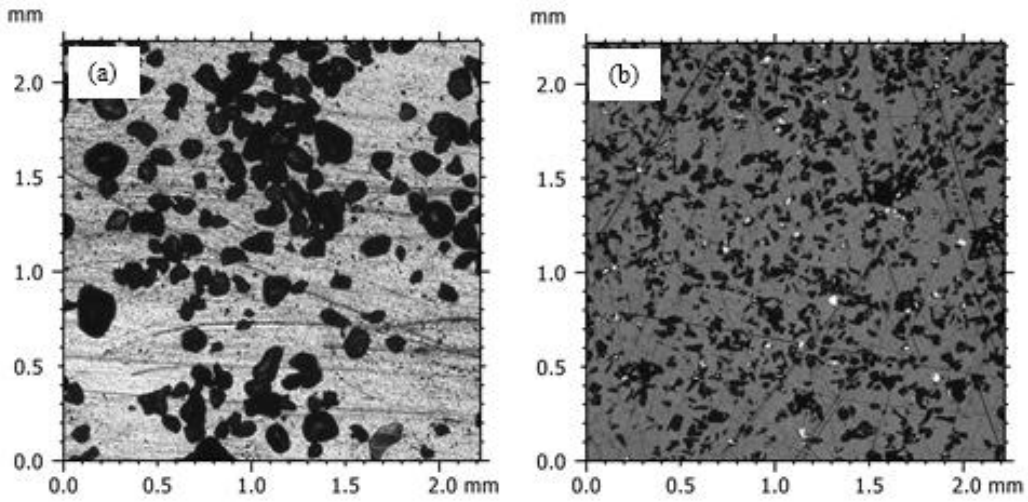

Figure 5.1: Reinforcing particles (a) dune sand and (b) silicon carbide.

The average size of voids in neat PLA filaments was measured using cross-sectional and longitudinal samples as 28 µm and 24 µm, respectively. After characterizing the voids in neat PLA filaments, it is easier to distinguish voids that were already inside the filament from the voids that result from particles dislodged during the polishing process. In Figures 5.2 and 5.3, voids, probable void locations, particle and probable particle locations are highlighted to have a better view of reinforcement distribution inside the filament. Figures showing microscopic of circular samples such as Figure 5.3 (a) represent a cross-sectional view of the filament while the figures that show rectangular samples like Figure 5.3 (b) represent a longitudinal section of the filament. The boundaries of the filament sectioned specimens can be distinguished visually from the cold mould by colour or visible surface topography.

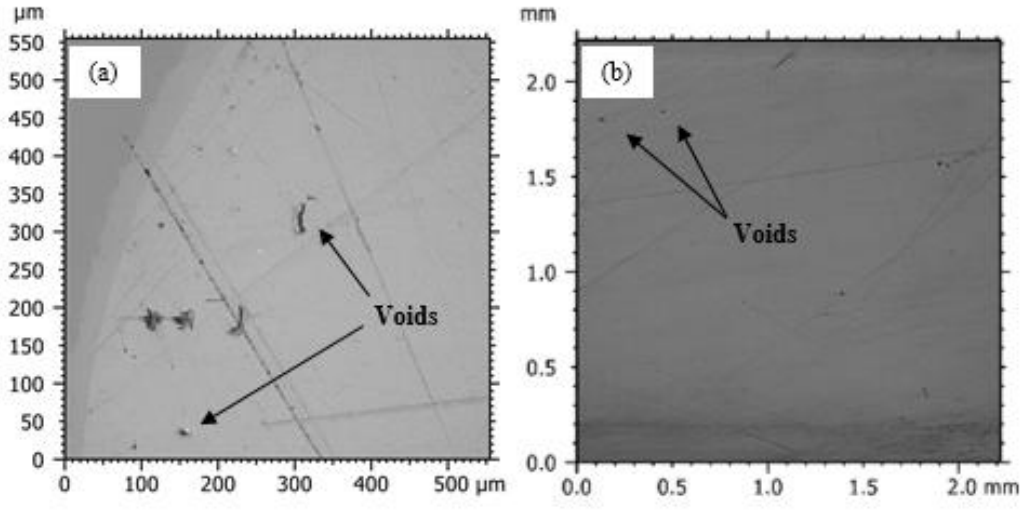

Figure 5.2: Voids in (a) cross and (b) longitudinal sections of neat PLA filament.

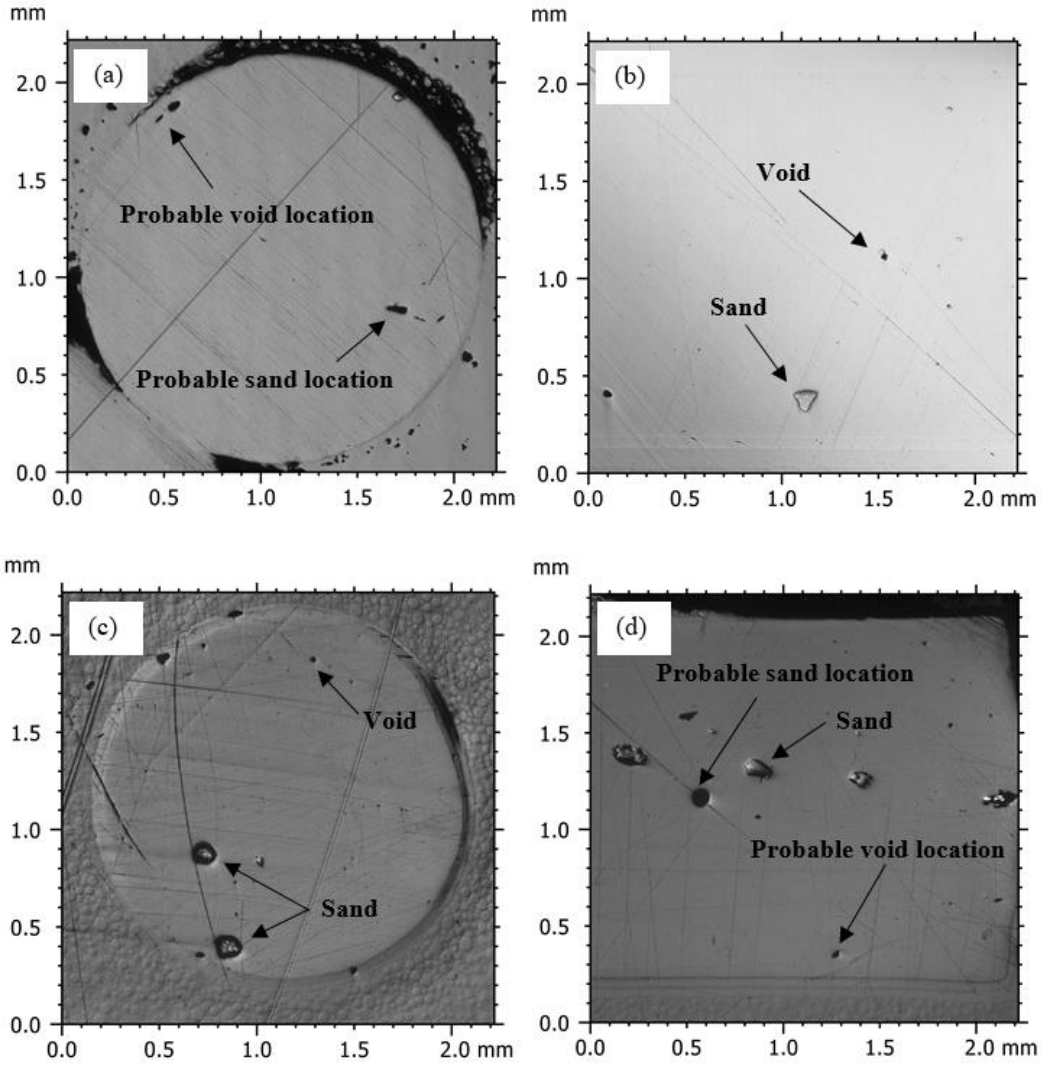

Figure 5.3: Material voids, sand-induced voids due to polishing and sand particles for (a)~(b) 0.5 wt% sand and (c)~(d) 2 wt% sand in PLA.

Low reinforcement quantity can indicate how far a particle can penetrate into the fabricated polymeric filament; however, it is not an indicator of how well the particles are dispersed inside the filament. Therefore, to have a better insight into the distribution of reinforcing particles in the filament, composites with higher weight percentage of reinforcement must be considered.

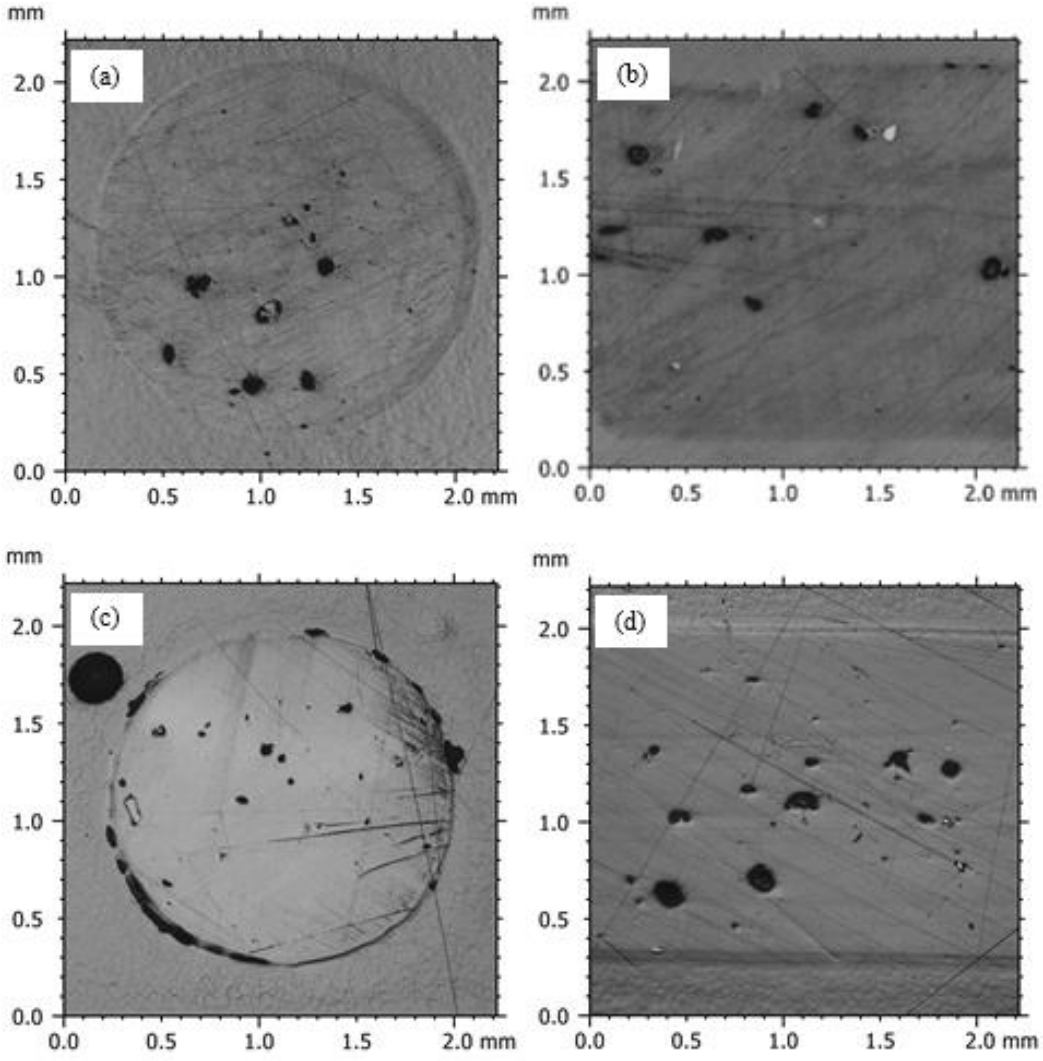

Figure 5.4: Cross-sectional and longitudinal view of (a)~(b) 3 wt% sand and (c)~(d) 4 wt% sand in PLA.

As more particles are dislodged during the polishing phase, it becomes harder to maintain a clean polish of the sample. This issue is encountered due to the abrasive nature of sand. Higher weight pecentage of reinfrocement are strong indicators of how well the reinforcement is distributed in the matrix. Figure 5.5 shows microscope images of 10 wt% and 15 wt% PLA-sand filaments. Despite the large quantity of sand present in the polymer, the distribution of sand is fairly divided between the center of the

filament as well as the areas near the surface. As a result, it can be concluded that the developed method serves as an adequate method of mixing and fabricating particle reinforced filaments with inorganic fillers.

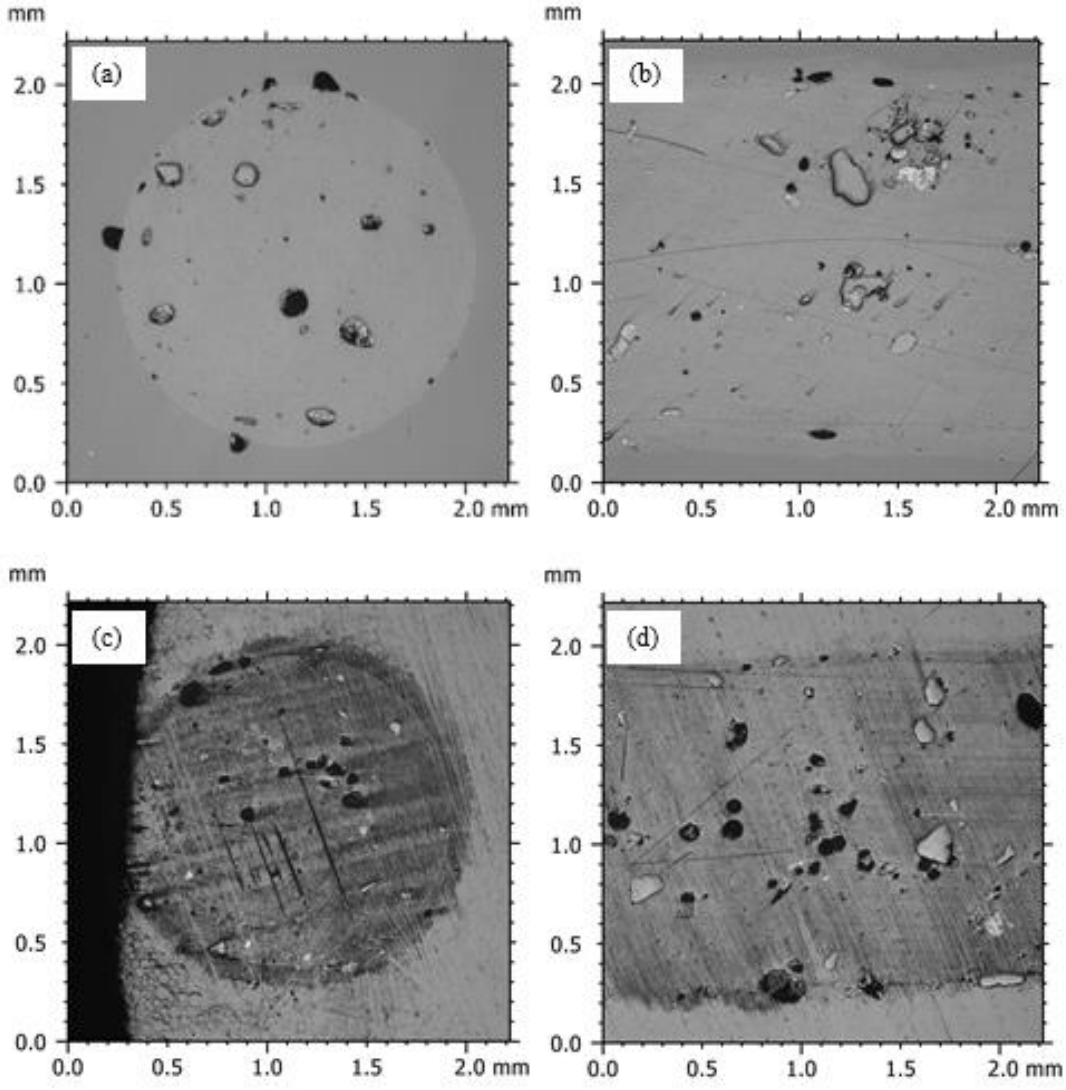

Figure 5.5: Microscopic images for (a)~(b) 10 wt% sand and (c)~(d) 15 wt% sand in PLA.

It is more challenging to capture clear and polished microscopic images for PLA-SiC filament due to higher quantity of abrasive SiC particles compared to sand particles. Figure 5.6 shows the distribution of SiC particles in 2 wt% PLA-SiC filament. Figure 5.6 (a) appears to have empty spaces that were occupied with SiC reinforcing particles. Several lines of scratches originate from void locations extending the ends of the specimen. These lines indicate that there were abrasive particles, namely SiC particles, filling these voids which tend to move out due to polishing process.

Comparing the dispersion of the reinforcing particles between the cases of 2 wt% PLA-SiC and 2 wt% PLA-sand shows that the SiC particles are more dispersed. SiC particles are smaller than sand particles, almost 1/3 of the size of sand particles, and therefore they tend to scatter more in the matrix resulting in better dispersion.

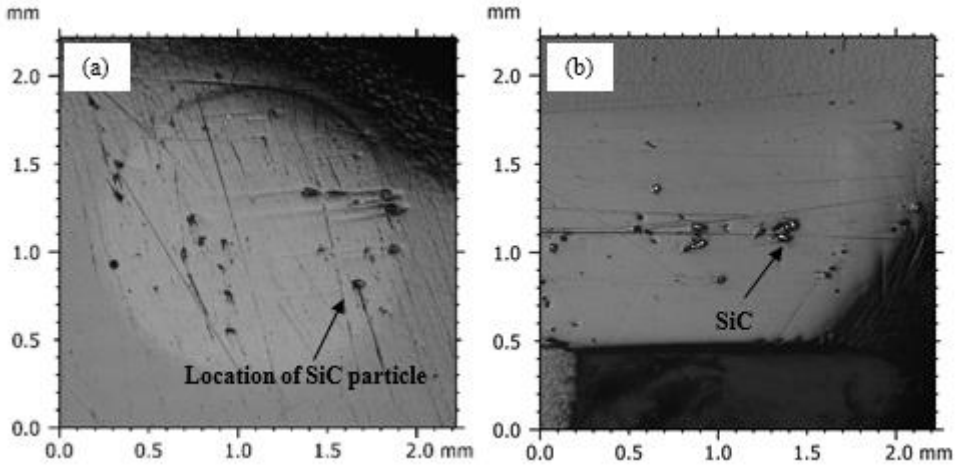

Figure 5.6: (a) cross-sectional and (b) longitudinal view of 2 wt% PLA-SiC filament.

SEM images of reinforcing particles inside the polymeric filament can give an insight on how well the reinforcing particles sit inside the polymeric material. Sand and SiC reinforcing particles shown in Figure 5.7 are located inside the sectioned filaments.

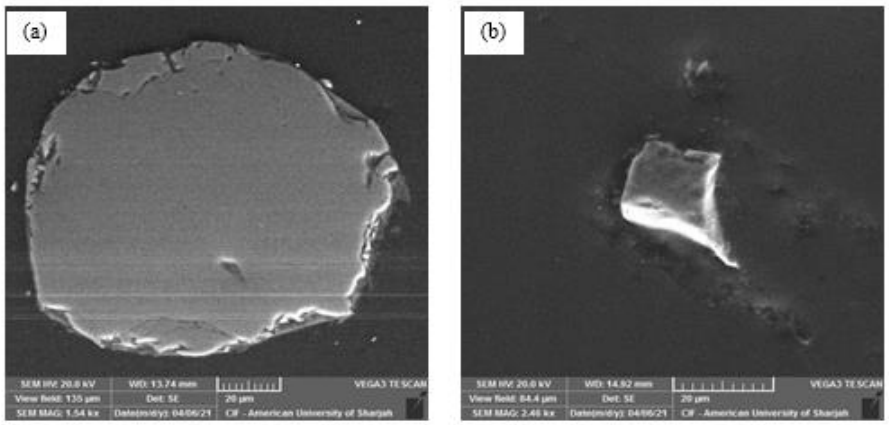

Figure 5.7: SEM images for (a) sand and (b) SiC particle in PLA.

The sand particle has a flat surface which is caused by multiple grinding and polishing passes to obtain a sectioned filament. Therefore, it can be concluded that there is a strong bonding between the reinforcing particles and polymeric material which is capable of keeping the particles in place and not dislodge out due to other external forces that result from filament sectioning process. As a result, SEM investigation further validates the developed method of mixing.

5.2. Tensile Response of PLA-Sand Composite Filaments

Mechanical characteristics of the developed PLA-sand filaments are assessed by analysing their stress-strain curve as shown in the sub-figures of Figure 5.8.

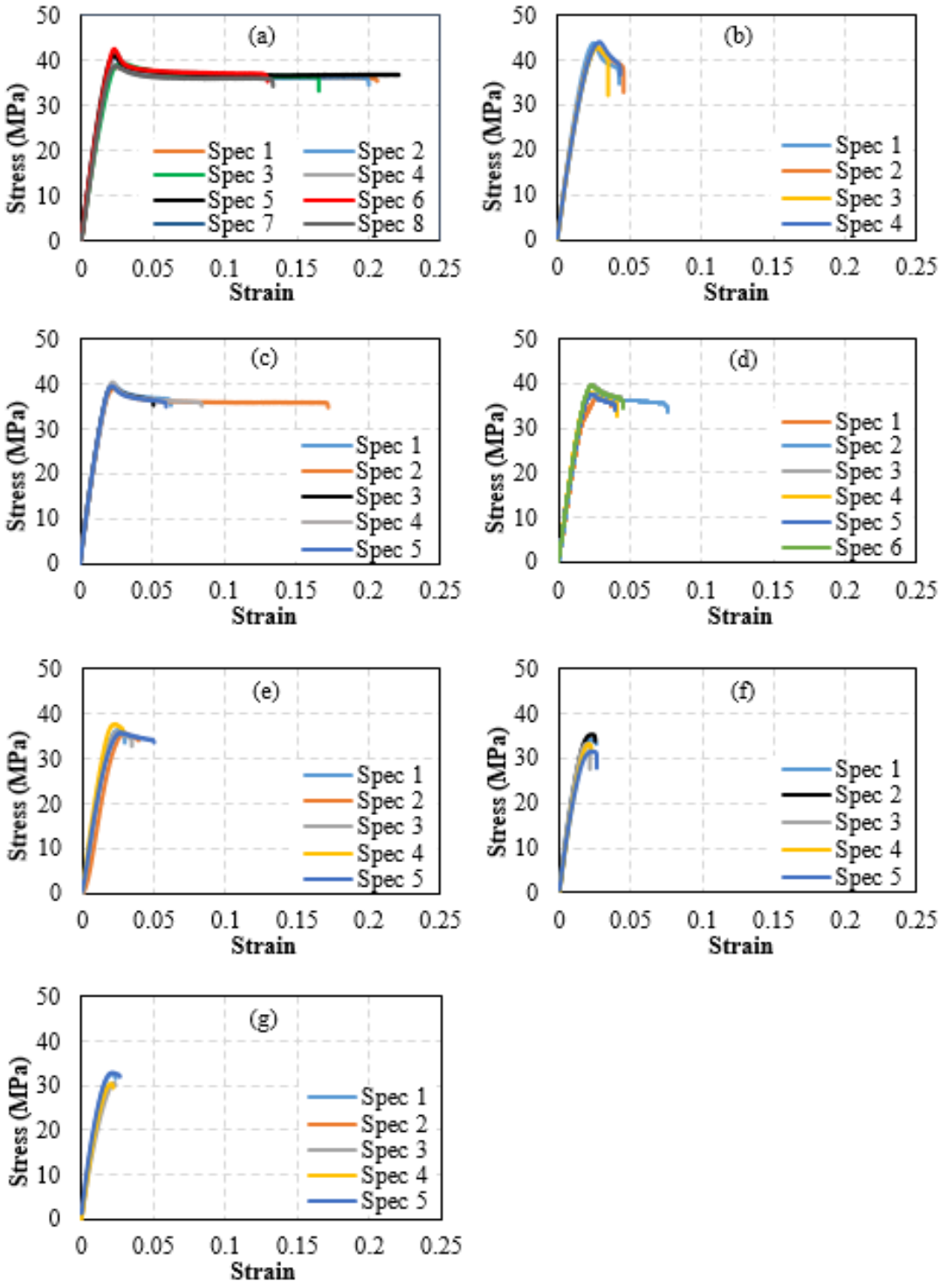

Figure 5.8: Stress-Strain curves of PLA filaments reinforced with fine dune sand. Subfigures (a)~(g) correspond to the sand weight fractions of 0%, 0.5%, 2%, 3% 4%, 10% and 15%, respectively.

5.2.1. Brittleness. Before characterizing the composite and analysing the mechanical response, harmony between the specimens of a given composite is noticed in exhibiting a relatively similar response which is one of the indicators for the effectiveness of the mixing method. To compare the stress-strain curves with each other, a considerable increase in brittleness of the polymer is noticed with the increase in the weight percentage of the reinforcement, that is, sand. In fact, the location of failure indicates brittle fracture. This phenomenon can be explained by the large size of the sand particles. Large sand particle in the extruded filaments concentrates the internal stresses and assists in starting cracks. Some specimens showed much higher ductility than their counterparts within same group (made using the same reinforcement content) such as specimen number 2 in plot (c) of Figure 5.8. The increase in elongation can be related to the lack of presence of large particles. The presence of large reinforcing particles in a given cross-section can drastically increase the brittleness of composite filament and serve as the weakest location where fracture will probably take place. The composite ceases to show any plastic response beyond 4 wt% of sand. Figure 5.9 shows the location of failure during tensile loading for specimens having different sand content, namely 0 wt%, 0.5 wt%, 4 wt% and 15 wt%.

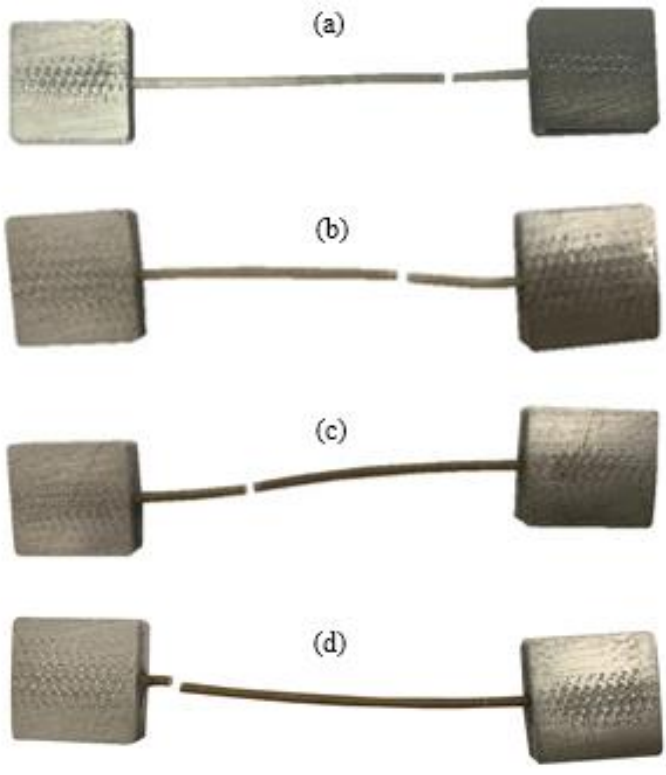

Figure 5.9: Failure location in tensile testing specimens for (a) 0 wt%, (b) 4 wt%, (c) 10 wt% and (d) 15 wt% sand in PLA.

5.2.2. Tensile strength. Ultimate tensile strength of PLA increased by 8%, from 40.0 MPa to 43.3 MPa with the addition of 0.5 wt% sand. Small amount of sand particles act like anchors that hold polymeric chains together, thus resulting in higher tensile strength. With further addition of reinforcement in the composite, that is 2 wt% sand, a decrease in tensile strength is noted compared to 0.5 wt%. Further increase in the reinforcement content beyond 2 wt% sand further decreased the filaments tensile strength as shown in Figure 5.10. The presence of a higher amount of large sand particles in a given cross-section acts like a large void or area of stress concentration which cause failure at that location. Regression is used to relate the ultimate tensile strength to sand weight percentage. Resulting relationship is shown in Figure 5.11.

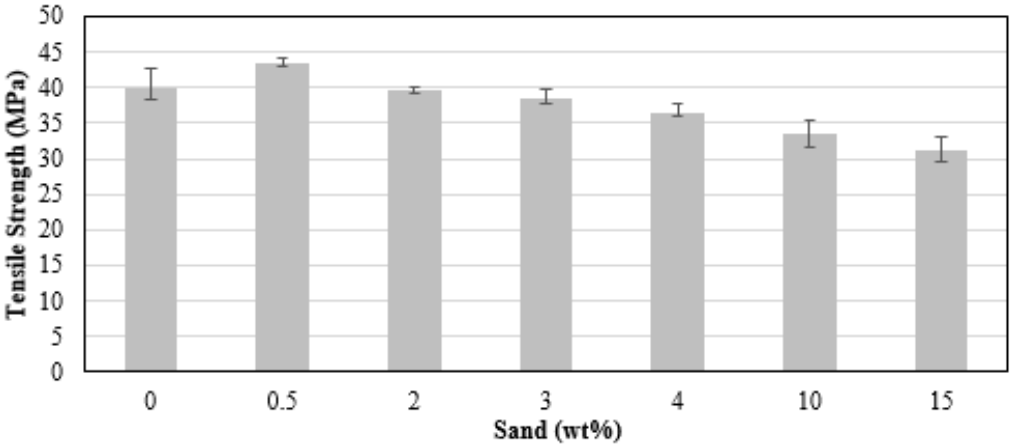

Figure 5.10: Ultimate tensile strength of PLA-sand composite filaments.

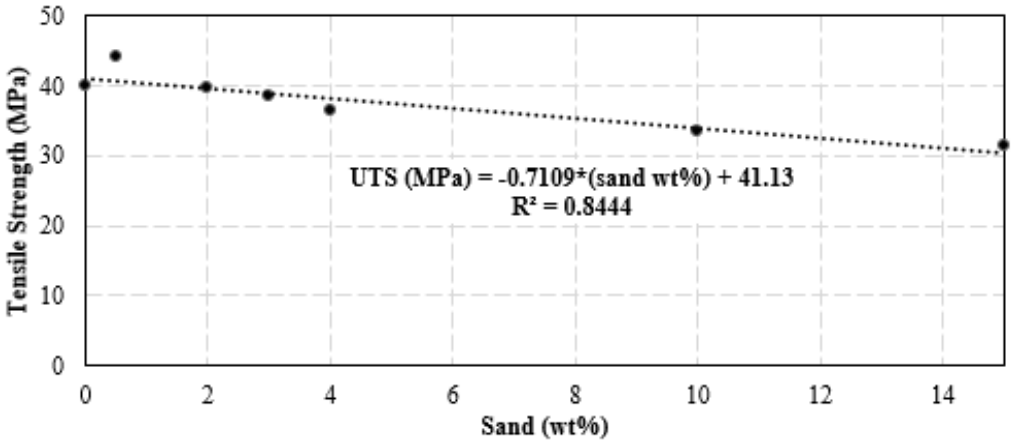

Figure 5.11: Linear correlation between ultimate tensile strength and sand wt%.

5.2.3. Stiffness. Another aspect of the assessment is the effect of sand content on stiffness. A slight improvement is noticed with 0.5 wt% sand; however, the highest stiffness was recorded at 2 wt% sand with an improvement of 4.5% compared to pure

PLA. Figure 5.12 shows the variation in stiffness with further addition of sand particles to the polymer. Further addition in sand content beyond 2 wt% leads to a decrease in stiffness of the filament.

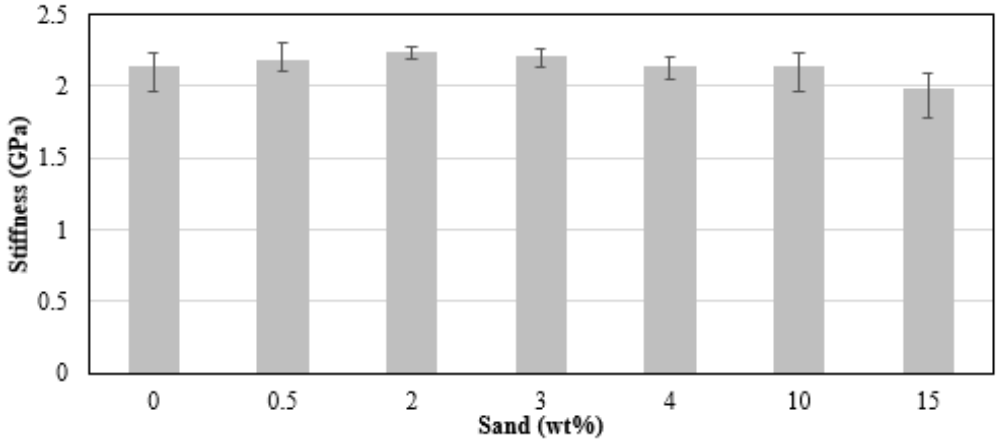

Figure 5.12: Stiffness of PLA-sand composite filaments.

5.3. PLA-Sand Composite in Compression

Figure 5.13 shows compression stress-strain curves for PLA-sand filaments.

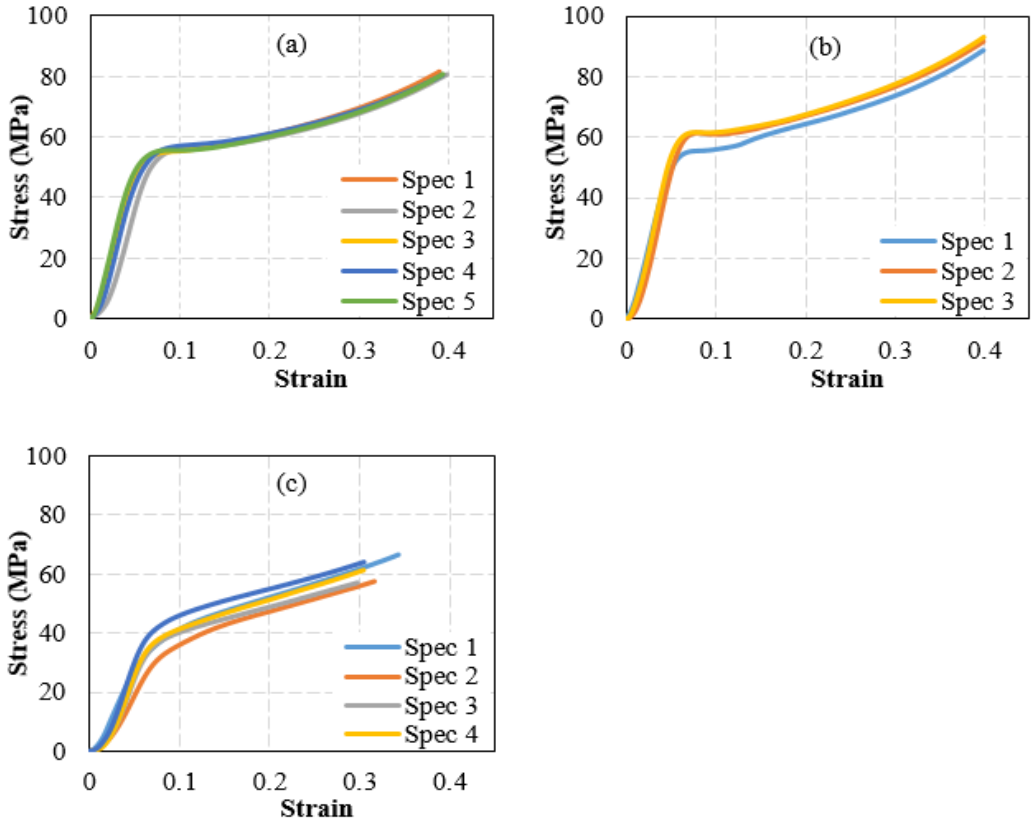

Figure 5.13: Stress-Strain curves of 3D printed PLA-sand compression specimens. Subfigures (a)~(c) correspond to the sand weight fractions of 0%, 0.5% and 15%, respectively.

The primary purpose of testing the composite in compression is to validate the printability of the developed reinforced filaments and study the effect of 3D printing on the mechanical response of the composite. To reduce material consumption and printing time, a small range of reinforced filaments was printed, which comprised 0 wt%, 0.5 wt% and 15 wt%. The compression test was automatically stopped at 4 mm displacement to cover the data of interest. Engineering stress-strain curves resulting from different specimens having the same weight fraction of reinforcements show considerable agreement. This indicates that the specimens have consistent composition and indicates that the mixing process proposes is efficient in dispersing the reinforcing particles.

5.3.1. Yield strength. The addition of 0.5 wt% sand slightly improved the yield strength of PLA-sand composite filaments compared to pure PLA as shown in the Figure 5.14.

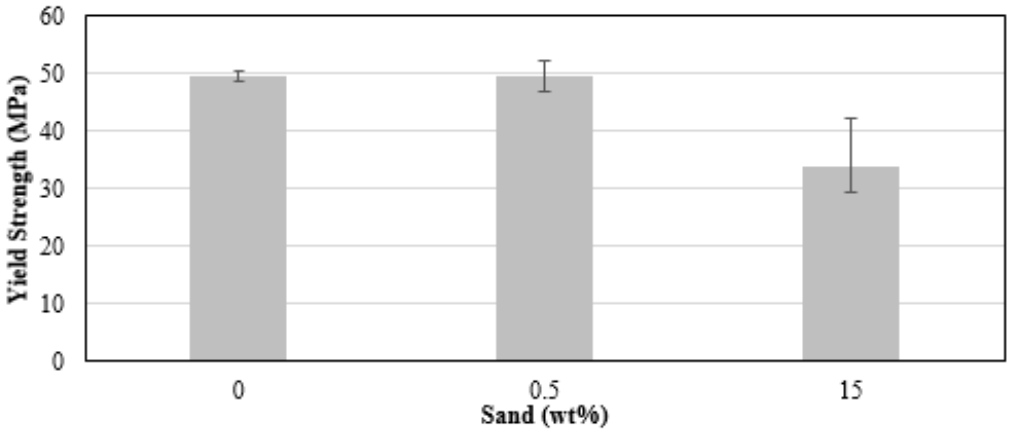

Figure 5.14: Yield strength of 3D printed PLA-sand compression specimens.

Although the maximum yield strength was recorded at 0.5 wt% sand among the tested group (0 wt%, 0.5 wt% and 15 wt%), there could be a higher increase in yield strength with sand content between 0.5 wt% and 15 wt%; however, due to limitations on time and material, it was decided to jump to 15 wt% sand and move the investigation to another reinforcing material as it will be discussed later in this report. The yield strength was decreased by more than 30% for the case of 15 wt% sand reinforcement compared to that of pure PLA. Therefore, high sand weight fraction such as 15 wt% in PLA leads to faster plastic deformation under lower load carrying capacity compared to neat PLA and 0.5 wt% PLA-sand composite.

5.3.2. Stiffness. The stiffness of 3D printed neat PLA is higher in tension than in compression. However, it is difficult to compare the compressive results to the tensile results in this study and the compressive results are for 3D printed specimens. Compression samples were fabricated using 3D printing and therefore they may include more voids and have weaker interlayer adhesion between their printed layers. For the compressed specimens, the maximum stiffness was observed at 0.5 wt% sand as seen in Figure 5.15. It was higher by 5% as compared to pure PLA. However, increasing the reinforcing sand content to 15wt% reduced the stiffness by 34%.

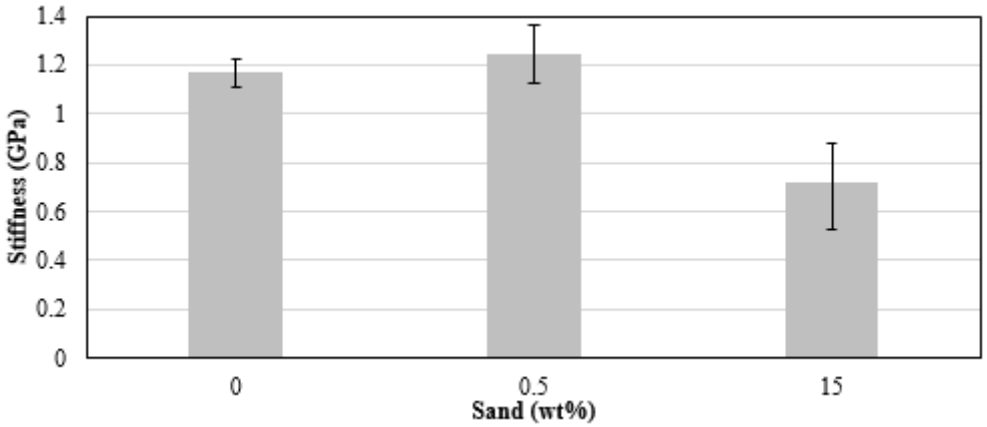

Figure 5.15: Stiffness of 3D printed PLA-sand compression specimens.

Based on the aforementioned results, it can be concluded that the addition of sand beyond 0.5 wt% has a negative impact on the mechanical performance of the composite. Large sand particles could be the major parameter that negatively affect the mechanical properties of the polymeric filaments at higher sand contents. The next set of composite filaments has smaller particulate size. The same preparation and testing methods that were applied to PLA-sand composite filaments are applied to the PLA-SiC filaments.

5.4. Tensile Response of PLA-SiC Composite Filaments

The effect of Silicon carbide particles on the performance of PLA-SiC composites filaments were investigated. PLA-SiC filaments were fabricated once the PLA-sand filaments were tested. PLA pellets used to fabricate PLA-SiC filaments are from the same PLA batch that was used to fabricate the PLA-sand filaments. However, as the two types reinforced filaments were fabricated at different times, the PLA constituent in each of them may exhibit different mechanical properties. This can be related to PLA pellets aging. Accordingly, in addition to testing PLA-SiC filaments,

tests were performed on neat PLA samples. The latter should give insights into the level of aging and its effect on PLA. Figure 5.16 shows the stress-strain curves for 0 wt%, 0.5 wt%, 1 wt%, 1.5 wt% and 2 wt% PLA-SiC PLA-SiC filaments. Similar to PLA-sand composites, PLA-SiC composites demonstrate uniformity in their stress-strain response. This indicates that the developed mixing method is effective in dispersing the SiC particles and capable of fabricating filaments reinforced with inorganic fillers.

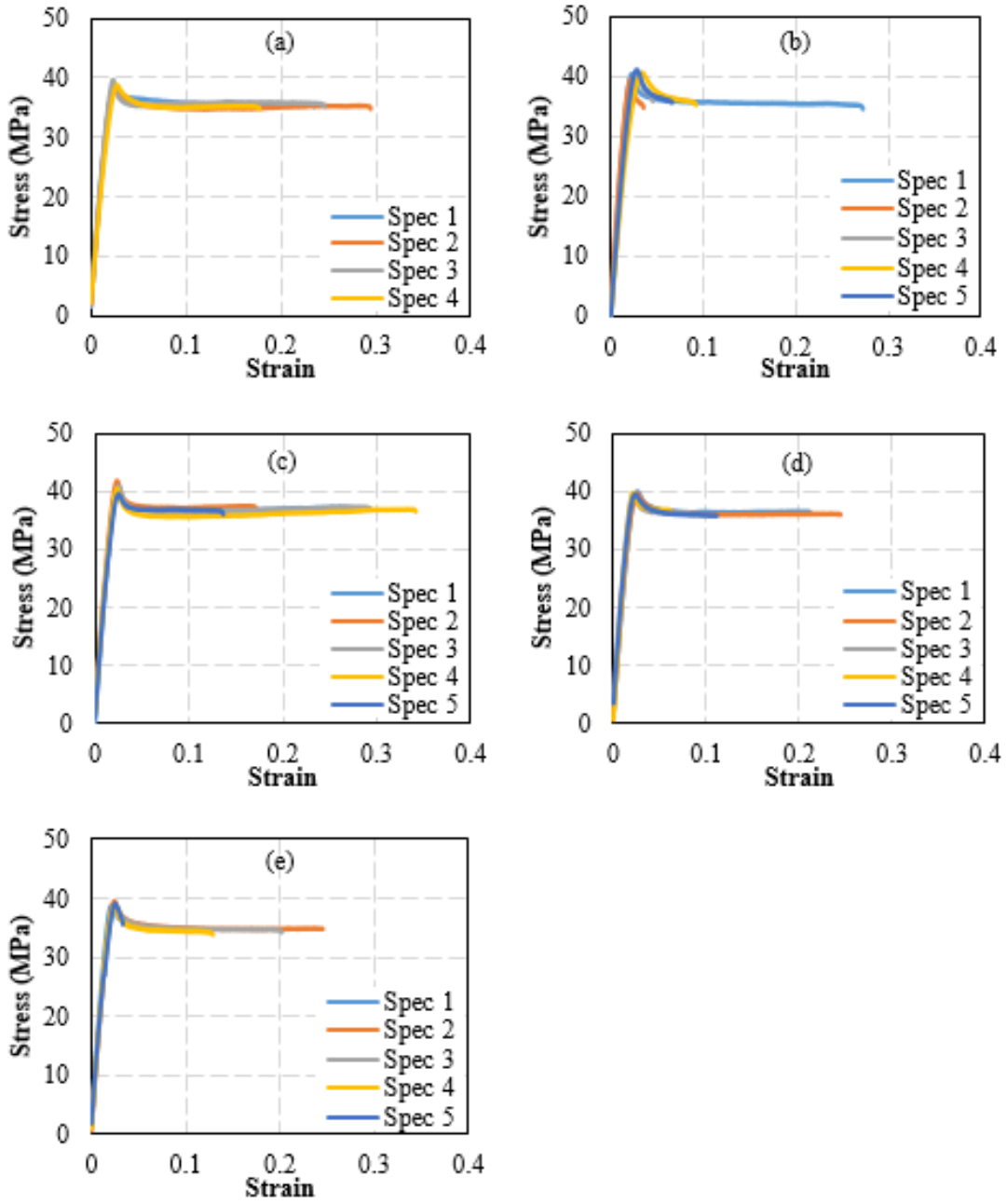

Figure 5.16: Stress-Strain curves of PLA filaments reinforced with SiC. Subfigures (a)~(e) correspond to the SiC weight fractions of 0%, 0.5%, 1%, 1.5% and 2%, respectively.

5.4.1. Brittleness. Unlike PLA-sand composite filaments, stress-strain curves for PLA-SiC composite filaments showed significant scatter in their failure strain. Variation in the failure strain among samples with the same composition could be due variation in void content and size present in the samples. Figure 5.17 shows the failure location developed in specimens subjected to the tensile testing protocol. Failure is located far away from the supports. No apparent necking or notable reduction in area were observed, which indicated that the material failed in a brittle manner.

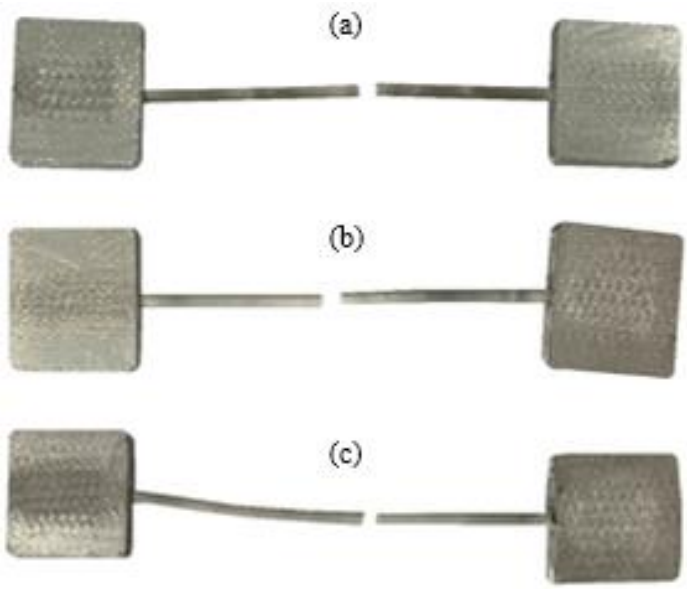

Figure 5.17: Failure location in tensile testing specimens for (a) 0.5 wt%, (b) 1 wt% and (c) 2 wt% SiC in PLA.

5.4.2. Tensile strength. Due to the nature of aging of PLA, the tensile strength of neat PLA was decreased by 3% as compared to that of the PLA used in PLA-sand filaments. Aging occurred during the course of approximately 600 hours, which is the approximate time period between when the PLA-sand filaments were tested and PLA-SiC filaments were fabricated. Unlike PLA-sand filaments, the maximum yield strength was observed at 1 wt% SiC. At this composition, the tensile strength improved by 5% as compared to that of pure PLA. Although the 1 wt% composition delivered the highest tensile strength (40.7 MPa), 0.5 wt% composition delivered a very close value (40.5 MPa). Beyond 1.5 wt% reinforcement, a notable decrease in the tensile strength values is observed. To better visualize the effect of SiC content in PLA, a second order polynomial correlation between SiC weight percentage and the ultimate tensile strength has been plotted for PLA-SiC reinforced filaments in Figure 5.19.

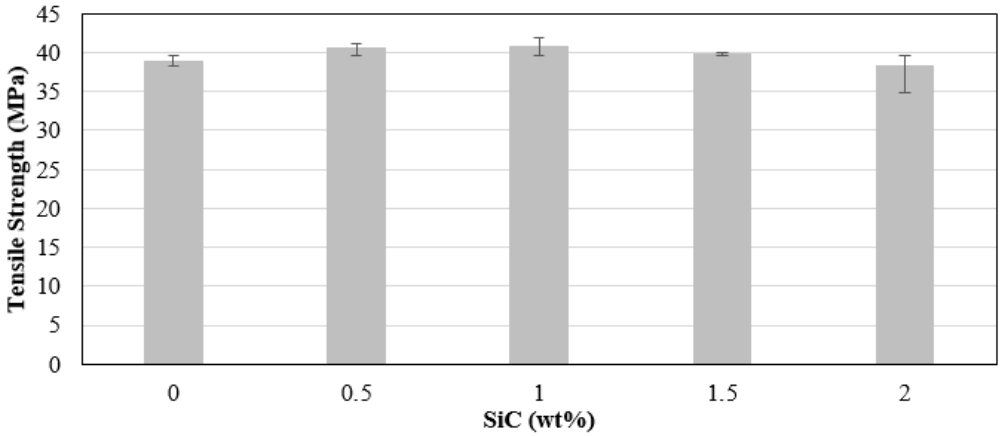

Figure 5.18: Ultimate tensile strength of PLA-SiC composite filaments.

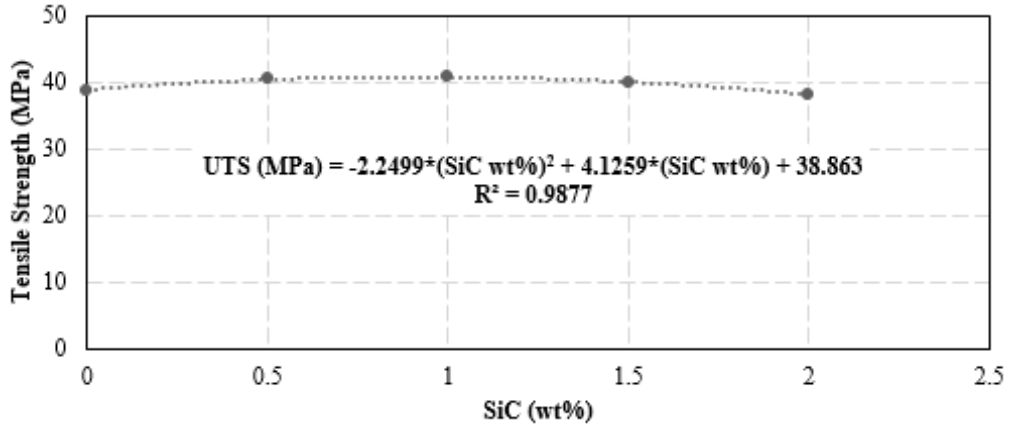

Figure 5.19: Second order correlation between ultimate tensile strength and SiC wt%.

5.4.3. Stiffness. After 600 hours, the stiffness of neat PLA was reduced by 10% as seen in Figure 5.20. Despite the minor differences in stiffness of PLA-SiC filaments, 1 wt% PLA-SiC has the highest averaged stiffness, 9% higher than that of neat PLA. Regardless of the quantity of reinforcing particles, if the weight percentage is between 0.5 wt% and 2 wt% of the overall composite, it will have a positive effect on stiffness.

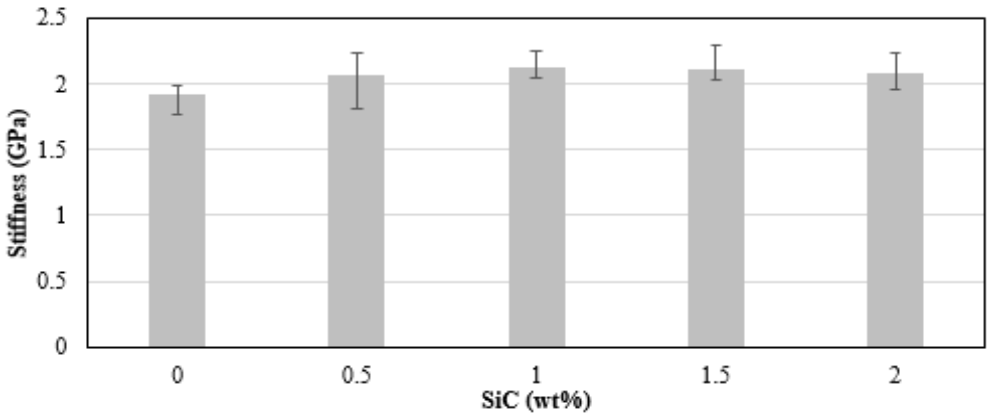

Figure 5.20: Stiffness of PLA-SiC composite filaments.

5.5. PLA-SiC Composite in Compression

Figure 5.21 shows the stress-strain curves for 3D printed PLA-SiC composite. Like PLA-sand, compression samples were printed to validate the printability of the fabricated PLA-SiC filament and study the effect of 3D printing on the properties of the filament.

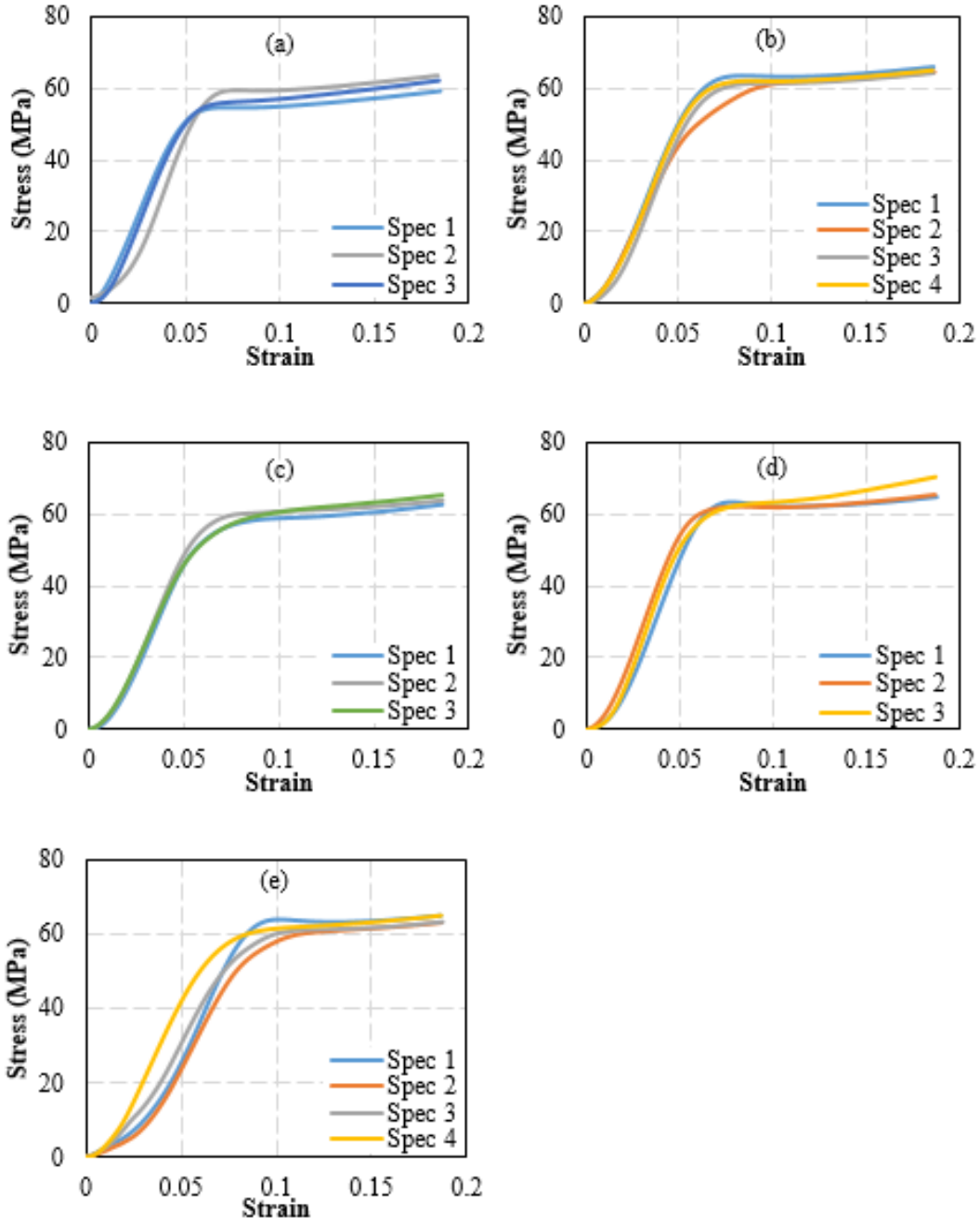

Figure 5.21: Stress-Strain curves of 3D printed PLA-SiC compression specimens. Subfigures (a)~(e) correspond to the SiC weight fractions of 0%, 0.5%, 1%, 1.5% and 2%, respectively.

5.5.1. Yield strength. Compressive properties of neat PLA were also affected by aging. Yield strength was increased by 4% which constitutes to approximately 1 MPa after 600 hours of aging.

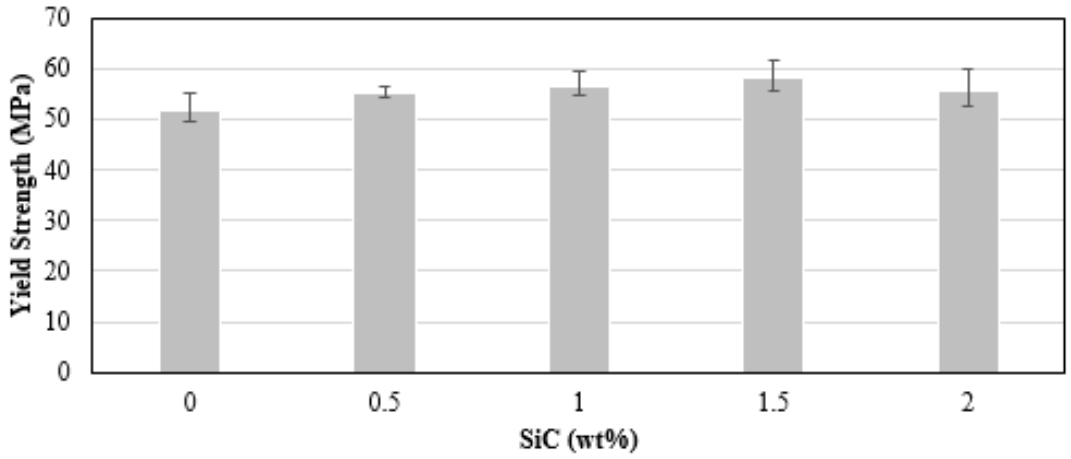

Figure 5.22: Yield strength of 3D printed PLA-SiC compression specimens.

The increase in yield strength can be explained by the hydrogenic behaviour of PLA which will be further explained in Section 5.6 of this report. As shown in Figure 5.22, 1.5 wt% SiC has the maximum yield strength. This maximum value is 6 MPa higher than that of neat PLA. As a result, 1.5 wt% of SiC reinforcement was capable of raising the yield strength by almost 12%. This indicates that reinforcing PLA with SiC enables the composite to withstand considerably higher loads.

5.5.2. Stiffness. After 600 hours, compression testing showed that the stiffness of PLA was decreased by almost 10%.

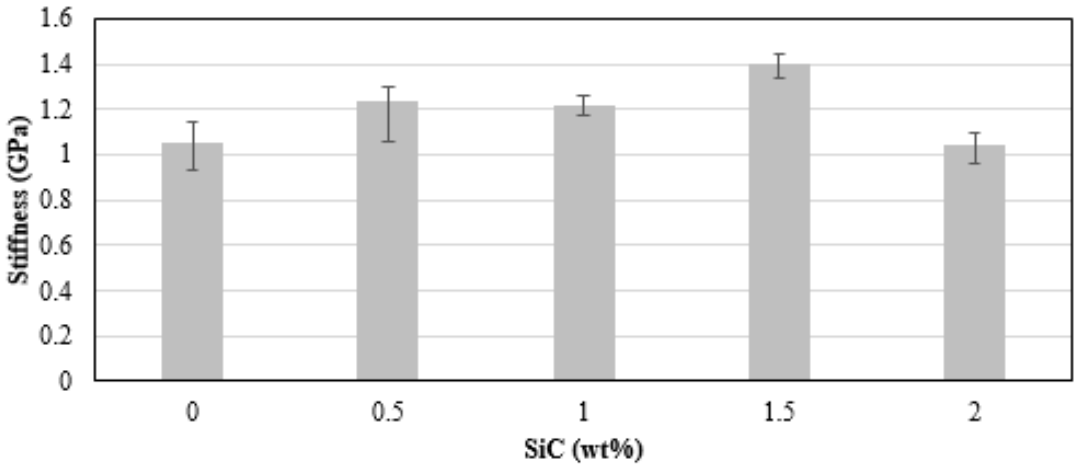

Figure 5.23: Stiffness of 3D printed PLA-SiC compressions samples.

The addition of 0.5 wt% and 1 wt% SiC reinforcement increased the stiffness of the composite; however, both composites seem to have overlapping readings. Despite the overlap, there is a bigger chance of picking a specimen from 1 wt% SiC composite that has a higher stiffness than that of 0.5 wt%. This is concluded by looking at the error bars of 0.5 wt% and 1 wt% composites shown in the Figure 5.23. Maximum stiffness was recorded for 1.5 wt% PLA-SiC composite, which exhibited a 25% higher averaged stiffness as compared to pure PLA. On the other hand, 2 wt% SiC composite exhibited an averaged stiffness that approximately is equivalent to that of pure PLA.

5.6. Effect of Aging

To have a better insight into the effect of aging and humidity on the mechanical properties of neat PLA, a period of time was allocated for aging purpose before initiating the process of fabricating neat PLA and PLA-SiC filaments. PLA pellets were stored in sealed bags inside cabinets that were placed in a laboratory with standard room conditions. Room temperature was fluctuating between 22 ºC and 24 ºC whereas humidity levels were ranging between 50% and 55%. The time allocated between both fabrication processes was approximately 600 hours. Hydrolysis followed by microbial digestion are the key factors behind degradation of PLA. The effect of aging was analysed through testing neat PLA before and after the aging time and comparing the results as shown in the Figure 5.24.

Tensile strength of neat PLA filaments was decreased from 40 MPa to 38.7 MPa after 600 hours of aging which could be related to weaker intermolecular bonds through scission of ester bonds into carboxylic acid and alcohol by chemical hydrolysis [62]. In fact, chemical hydrolysis is initiated by the addition of humidity to the polymer.

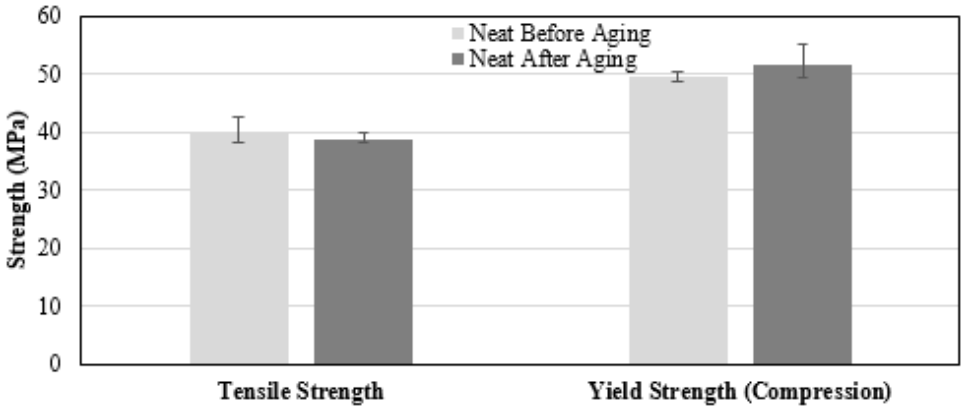

Figure 5.24: Effect of aging on tensile strength and yield strength of neat PLA.

On the other hand, compressive yield strength of 3D printed compression specimens seems to change slightly after aging. It only increased by 1 MPa which may be related to increased moisture content in the tested specimens. Stiffness, however, decreases with aging under tensile and compressive loading as shown in Figure 5.25. Therefore, aging has a negative impact on the tensile strength and stiffness of neat PLA as well as PLA composites. Higher yield strength under compression loading was the only improvement that was observed after aging.

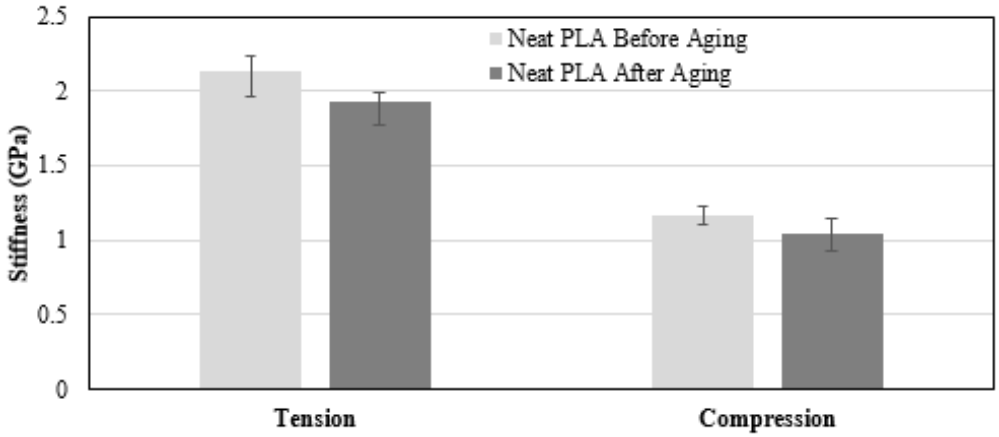

Figure 5.25: Effect of aging on stiffness of neat PLA.

Chapter 6. Conclusion and Future Work

This study proposes a low-cost process for the fabrication of filaments compatible with FDM 3D printers and reinforced with inorganic fillers. The proposed process utilizes a regular oven and a low cost single-screw extruder. In the proposed process, inorganic fillers are heated and deposited on plastic pellets. Subsequently, the pellets are converted to filaments using a single-screw desktop extruder. The low coast process opens doors for researchers as well as hobbyists to fabricate reinforced filaments using various types of reinforcements.

The effectiveness of the proposed fabrication method in mixing and dispersing the inorganic reinforcements was validated through a microscopic study. Longitudinal and cross-sectional specimens of PLA-sand and PLA-SiC filaments were examined. Microscopy images confirmed that the reinforcing particles dispersed properly inside the polymeric matrix. Smaller reinforcing particles exhibited better dispersion behaviour. The stress-strain curves of PLA-Sand and PLA-SiC filaments under axial tensile loading were measured. Stress-strain curves of samples having similar composition showed minimal scatter, indicating that the inorganic fillers were effectively distributed.

Mechanical characterization of the fabricated reinforced filaments was conducted by investigating their behaviour under tensile loadings. The highest tensile strength (8% higher than neat PLA) and stiffness (4.5% higher than neat PLA) for PLA-sand were observed at the compositions of 0.5 wt% and 2 wt% sand, respectively. The highest tensile strength (5% higher than neat PLA) and stiffness (9% higher than neat PLA) for PLA-SiC filaments were observed at the composition of 1 wt% SiC. Silicon carbide particles proved to be a better reinforcing filler for its small size and superior mechanical properties.

The compatibility of the produced reinforced filaments with commercial desktop printers was assessed by printing cylindrical samples using PLA-sand and PLA-SiC filaments. Printed cylinders were tested under compressive loading to assess the yield strength and stiffness. The highest yield strength and stiffness for PLA-sand and PLA-SiC composite were observed at the composition of 0.5 wt% sand and 1.5

wt% SiC, respectively. In general, yield strength and stiffness values were within the expected margins.

Effect of aging of PLA was explored by analysing the mechanical characteristics of neat PLA before and after 600 hours of aging. PLA undergoes aging due to its capability to biodegrade. Humidity is one of the key factors that accelerate biodegradation. Due to aging, the tensile strength of PLA filaments decreased by 3%. However, yield strength of 3D printed parts, from aged filaments, under compression loading increased by 4%. Stiffness of filaments and printed compression samples decreases with aging.

Future work will incorporate effect of environmental conditions on other mechanical characteristics of PLA. In addition, a low-cost desktop extruder will be designed and manufactured to automatically fabricate reinforced filaments with minimal human interference.

References

[1] L. J. Kumar, P. M. Pandey, and D. I. Wimpenny, *3D printing and additive manufacturing technologies*, vol. 311, pp. 1-9, 2019.

[2] M. Whitaker, "The history of 3D printing in healthcare," *The Bulletin of the Royal College of Surgeons of England*, vol. 96, pp. 228-229, 2014.

[3] M. Alkhader and M. Vural, "Mechanical response of cellular solids: Role of cellular topology and microstructural irregularity," *International Journal of Engineering Science*, vol. 46, pp. 1035-1051, 2008.

[4] M. Alkhader and M. Vural, "The partition of elastic strain energy in solid foams and lattice structures," *Acta Materialia*, vol. 57, pp. 2429-2439, 2009.

[5] M. Alkhader and M. Vural, "An energy-based anisotropic yield criterion for cellular solids and validation by biaxial FE simulations," *Journal of the Mechanics and Physics of Solids*, vol. 57, pp. 871-890, 2009.

[6] M. Alkhader and M. Vural, "A plasticity model for pressure-dependent anisotropic cellular solids," *International Journal of Plasticity*, vol. 26, pp. 1591-1605, 2010.

[7] M. Alkhader, M. Nazzal, and K. Louca, "Design of bending dominated lattice architectures with improved stiffness using hierarchy," *Proceedings of the Institution of Mechanical Engineers Part C-Journal of Mechanical Engineering Science*, vol. 233, pp. 3976-3993, Jun 2019.

[8] M. Alkhader, W. Abuzaid, M. Elyoussef, and S. Al-Adaileh, "Localized strain fields in honeycomb materials with convex and concaved cells," *European Journal of Mechanics - A/Solids*, vol. 80, p. 103890, 2020/03/01/ 2020.

[9] S. Iyer and T. A. Venkatesh, "Electromechanical response of porous piezoelectric materials: Effects of porosity connectivity," *Applied Physics Letters*, vol. 97, p. 072904, 08/16/ 2010.

[10] S. Iyer, M. Alkhader, and T. A. Venkatesh, "Electromechanical Response of Piezoelectric Honeycomb Foam Structures," *Journal of the American Ceramic Society*, vol. 97, pp. 826-834, Mar 2014.

[11] S. Iyer, M. Alkhader, and T. A. Venkatesh, "Electromechanical behavior of auxetic piezoelectric cellular solids," *Scripta Materialia*, vol. 99, pp. 65-68, Apr 1 2015.

[12] S. Iyer, M. Alkhader, and T. A. Venkatesh, "On the relationships between cellular structure, deformation modes and electromechanical properties of piezoelectric cellular solids," *International Journal of Solids and Structures*, vol. 80, pp. 73-83, Feb 2016.

[13] W. Abuzaid, M. Alkhader, and M. Omari, "Experimental analysis of heterogeneous shape recovery in 4d printed honeycomb structures," *Polymer Testing*, vol. 68, pp. 100-109, 2018/07/01/ 2018.

[14] M. H. Yousuf, W. Abuzaid, and M. Alkhader, "4D printed auxetic structures with tunable mechanical properties," *Additive Manufacturing*, vol. 35, p. 101364, 2020/10/01/ 2020.

[15] D. E. Henton, P. Gruber, J. Lunt, and J. Randall, "Polylactic acid technology," *Natural fibers, biopolymers, and biocomposites*, vol. 16, pp. 527-577, 2005.

[16] S. K. Vishwakarma, P. Pandey, and N. K. Gupta, "Characterization of ABS material: a review," *Journal of Research in Mechanical Engineering*, vol. 5, pp. 13-16, 2017.

[17] Z. Wei, R. Wang, C. Zhang, J. Wang, Y. Yang, W. Wang, *et al.*, "Preparation and characterization of super-toughened PA6/r-PVB blends with “transplanted” multicore morphology by reactive compatibilization," *European Polymer Journal,* vol. 143, p. 110173, 2021/01/15/ 2021.
[18] S. Ghatge, Y. Yang, J.-H. Ahn, and H.-G. Hur, "Biodegradation of polyethylene: a brief review," *Applied Biological Chemistry,* vol. 63, p. 27, 2020/05/16 2020.
[19] G. Skirbutis, A. Dzingutė, V. Masiliūnaitė, G. Šulcaitė, and J. Žilinskas, "A review of PEEK polymer’s properties and its use in prosthodontics," *Stomatologija,* vol. 19, pp. 19-23, 2017.
[20] A. Goyanes, M. Kobayashi, R. Martínez-Pacheco, S. Gaisford, and A. W. Basit, "Fused-filament 3D printing of drug products: Microstructure analysis and drug release characteristics of PVA-based caplets," *International Journal of Pharmaceutics,* vol. 514, pp. 290-295, 2016/11/30/ 2016.
[21] W. Yu, X. Wang, E. Ferraris, and J. Zhang, "Melt crystallization of PLA/Talc in fused filament fabrication," *Materials & Design,* vol. 182, p. 108013, 2019.
[22] C.-Y. Lee and C.-Y. Liu, "The influence of forced-air cooling on a 3D printed PLA part manufactured by fused filament fabrication," *Additive Manufacturing,* vol. 25, pp. 196-203, 2019.
[23] T. Rimpongpisarn, W. Wattanathana, K. Sukthavorn, N. Nootsuwan, Y. Hanlumyuang, C. Veranitisagul and A. Laobuthee, "Novel luminescent PLA/MgAl2O4: Sm3+ composite filaments for 3D printing application," *Materials Letters,* vol. 237, pp. 270-273, 2019.
[24] F. Daver, K. P. M. Lee, M. Brandt, and R. Shanks, "Cork–PLA composite filaments for fused deposition modelling," *Composites Science and Technology,* vol. 168, pp. 230-237, 2018.
[25] Y. Zhou, L. Lei, B. Yang, J. Li, and J. Ren, "Preparation and characterization of polylactic acid (PLA) carbon nanotube nanocomposites," *Polymer Testing,* vol. 68, pp. 34-38, 2018.
[26] F. Lopresti, F. C. Pavia, I. Vitrano, M. Kersaudy-Kerhoas, V. Brucato, and V. La Carrubba, "Effect of hydroxyapatite concentration and size on morpho-mechanical properties of PLA-based randomly oriented and aligned electrospun nanofibrous mats," *Journal of the mechanical behavior of biomedical materials,* vol. 101, p. 103449, 2020.
[27] E. A. Papon and A. Haque, "Fracture toughness of additively manufactured carbon fiber reinforced composites," *Additive Manufacturing,* vol. 26, pp. 41-52, 2019.
[28] N. Ayrilmis, "Effect of layer thickness on surface properties of 3D printed materials produced from wood flour/PLA filament," *Polymer testing,* vol. 71, pp. 163-166, 2018.
[29] V. D. P. Rao, P. Rajiv, and V. N. Geethika, "Effect of fused deposition modelling (FDM) process parameters on tensile strength of carbon fibre PLA," *Materials Today: Proceedings,* vol. 18, pp. 2012-2018, 2019.
[30] Z. Wang, J. Xu, Y. Lu, L. Hu, Y. Fan, J. Ma, *et al.*, "Preparation of 3D printable micro/nanocellulose-polylactic acid (MNC/PLA) composite wire rods with high MNC constitution," *Industrial Crops and Products,* vol. 109, pp. 889-896, 2017.

[31] K. Fayazbakhsh, M. Movahedi, and J. Kalman, "The impact of defects on tensile properties of 3D printed parts manufactured by fused filament fabrication," *Materials Today Communications,* vol. 18, pp. 140-148, 2019.
[32] M. Q. Ansari, A. Redmann, T. A. Osswald, M. J. Bortner, and D. G. Baird, "Application of thermotropic liquid crystalline polymer reinforced acrylonitrile butadiene styrene in fused filament fabrication," *Additive Manufacturing,* vol. 29, p. 100813, 2019.
[33] V. Tambrallimath, R. Keshavamurthy, D. Saravanabavan, P. G. Koppad, and G. P. Kumar, "Thermal behavior of PC-ABS based graphene filled polymer nanocomposite synthesized by FDM process," *Composites Communications,* vol. 15, pp. 129-134, 2019.
[34] H. K. Sezer and O. Eren, "FDM 3D printing of MWCNT re-inforced ABS nano-composite parts with enhanced mechanical and electrical properties," *Journal of Manufacturing Processes,* vol. 37, pp. 339-347, 2019.
[35] D. Hwang and D. Cho, "Fiber aspect ratio effect on mechanical and thermal properties of carbon fiber/ABS composites via extrusion and long fiber thermoplastic processes," *Journal of Industrial and Engineering Chemistry,* vol. 80, pp. 335-344, 2019.
[36] M. Nikzad, S. Masood, and I. Sbarski, "Thermo-mechanical properties of a highly filled polymeric composites for fused deposition modeling," *Materials & Design,* vol. 32, pp. 3448-3456, 2011.
[37] C. Oztan, S. Ballikaya, U. Ozgun, R. Karkkainen, and E. Celik, "Additive manufacturing of thermoelectric materials via fused filament fabrication," *Applied Materials Today,* vol. 15, pp. 77-82, 2019.
[38] F. Castles, D. Isakov, A. Lui, Q. Lei, C. Dancer, Y. Wang, *et al.,* "Microwave dielectric characterisation of 3D-printed BaTiO 3/ABS polymer composites," *Scientific reports,* vol. 6, pp. 1-8, 2016.
[39] D. Isakov, Q. Lei, F. Castles, C. Stevens, C. Grovenor, and P. Grant, "3D printed anisotropic dielectric composite with meta-material features," *Materials & Design,* vol. 93, pp. 423-430, 2016.
[40] R. Singh, P. Bedi, F. Fraternali, and I. Ahuja, "Effect of single particle size, double particle size and triple particle size Al2O3 in Nylon-6 matrix on mechanical properties of feed stock filament for FDM," *Composites Part B: Engineering,* vol. 106, pp. 20-27, 2016.
[41] A. D. Pertuz, S. Díaz-Cardona, and O. A. González-Estrada, "Static and fatigue behaviour of continuous fibre reinforced thermoplastic composites manufactured by fused deposition modelling technique," *International Journal of Fatigue,* vol. 130, p. 105275, 2020.
[42] J. Tan and H. Low, "Embedded electrical tracks in 3D printed objects by fused filament fabrication of highly conductive composites," *Additive Manufacturing,* vol. 23, pp. 294-302, 2018.
[43] X. García-Fonte, A. Ares-Pernas, C. Cerecedo, V. Valcárcel, and M. J. Abad, "Influence of phase morphology on the rheology and thermal conductivity of HDPE/PA6 immiscible blends with alumina whiskers," *Polymer Testing,* vol. 71, pp. 56-64, 2018.
[44] C. G. Schirmeister, T. Hees, E. H. Licht, and R. Muelhaupt, "3D printing of high density polyethylene by fused filament fabrication," *Additive Manufacturing,* vol. 28, pp. 152-159, 2019.

[45] J.-Z. Liang, "Melt strength and drawability of HDPE, LDPE and HDPE/LDPE blends," *Polymer Testing,* vol. 73, pp. 433-438, 2019.
[46] B. Patil, B. B. Kumar, S. Bontha, V. K. Balla, S. Powar, V. H. Kumar, *et al.*, "Eco-friendly lightweight filament synthesis and mechanical characterization of additively manufactured closed cell foams," *Composites Science and Technology,* vol. 183, p. 107816, 2019.
[47] D. Gregor-Svetec, M. Leskovšek, U. V. Brodnjak, U. S. Elesini, D. Muck, and R. Urbas, "Characteristics of HDPE/cardboard dust 3D printable composite filaments," *Journal of Materials Processing Technology,* vol. 276, p. 116379, 2020.
[48] P. Geng, J. Zhao, W. Wu, W. Ye, Y. Wang, S. Wang, *et al.*, "Effects of extrusion speed and printing speed on the 3D printing stability of extruded PEEK filament," *Journal of Manufacturing Processes,* vol. 37, pp. 266-273, 2019.
[49] A. Golbang, E. Harkin-Jones, M. Wegrzyn, G. Campbell, E. Archer, and A. McIlhagger, "Production and characterization of PEEK/IF-WS2 nanocomposites for additive manufacturing: Simultaneous improvement in processing characteristics and material properties," *Additive Manufacturing,* vol. 31, p. 100920, 2020.
[50] C. Basgul, T. Yu, D. W. MacDonald, R. Siskey, M. Marcolongo, and S. M. Kurtz, "Does annealing improve the interlayer adhesion and structural integrity of FFF 3D printed PEEK lumbar spinal cages?," *Journal of the mechanical behavior of biomedical materials,* vol. 102, p. 103455, 2020.
[51] M. Hasan, C. Cherif, A. Foisal, T. Onggar, R. Hund, and A. Nocke, "Development of conductive coated Polyether ether ketone (PEEK) filament for structural health monitoring of composites," *Composites science and technology,* vol. 88, pp. 76-83, 2013.
[52] K. Bertoldi, V. Vitelli, J. Christensen, and M. van Hecke, "Flexible mechanical metamaterials," *Nature Reviews Materials,* vol. 2, p. 17066, 2017.
[53] M. Mohsenizadeh, F. Gasbarri, M. Munther, A. Beheshti, and K. Davami, "Additively-manufactured lightweight Metamaterials for energy absorption," *Materials & Design,* vol. 139, pp. 521-530, 2018/02/05/ 2018.
[54] S. Iyer, M. Alkhader, and T. A. Venkatesh, "Band Gaps in Bravais Lattices Inspired Periodic Cellular Materials and the Effect of Relative Density and Strain Fields," p. V013T16A022, 2014.
[55] M. Alkhader, S. Iyer, W. X. Shi, and T. A. Venkatesh, "Low frequency acoustic characteristics of periodic honeycomb cellular cores: The effect of relative density and strain fields," *Composite Structures,* vol. 133, pp. 77-84, Dec 1 2015.
[56] M. Alkhader, B. Abu-Nabah, M. Elyoussef, and T. A. Venkatesh, "Design of honeycomb structures with tunable acoustic properties," *MRS Advances,* vol. 4, pp. 2409-2418, 2019.
[57] A. Ahmed, M. Alkhader, and B. Abu-Nabah, "In-plane elastic wave propagation in aluminum honeycomb cores fabricated by bonding corrugated sheets," *Journal of Sandwich Structures & Materials,* vol. 21, pp. 2949-2974, Nov 2019.
[58] A. Ahmad, M. Alkhader, B. A. Abu-Nabah, and T. A. Venkatesh, "Effect of deformation mechanisms on in-plane wave propagation in periodic cellular materials," *Waves in Random and Complex Media,* pp. 1-23, 2021.

[59] S. Berretta, R. Davies, Y. Shyng, Y. Wang, and O. Ghita, "Fused Deposition Modelling of high temperature polymers: Exploring CNT PEEK composites," *Polymer Testing*, vol. 63, pp. 251-262, 2017.
[60] P. Wang, B. Zou, H. Xiao, S. Ding, and C. Huang, "Effects of printing parameters of fused deposition modeling on mechanical properties, surface quality, and microstructure of PEEK," *Journal of Materials Processing Technology*, vol. 271, pp. 62-74, 2019.
[61] M. K. J. E. Exconde, J. A. A. Co, J. Z. Manapat, and E. R. Magdaluyo Jr, "Materials selection of 3D printing filament and utilization of recycled polyethylene terephthalate (PET) in a redesigned breadboard," *Procedia CIRP*, vol. 84, pp. 28-32, 2019.
[62] C. Badouard, F. Traon, C. Denoual, C. Mayer-Laigle, G. Paës, and A. Bourmaud, "Exploring mechanical properties of fully compostable flax reinforced composite filaments for 3D printing applications," *Industrial Crops and Products*, vol. 135, pp. 246-250, 2019.
[63] Y. Tokiwa and B. P. Calabia, "Biodegradability and biodegradation of poly (lactide)," *Applied microbiology and biotechnology*, vol. 72, pp. 244-251, 2006.
[64] T. A. Khames Alsheriani, "Composition and Environmental Assessment of Soils from United Arab Emirates," pp. 74-78, 1998.

Vita

Mohamed Hassanien was born in 1994, in Dubai, United Arab Emirates. He received his primary and secondary education in Dubai, UAE. He received his B.Sc. degree in Mechanical Engineering from the American University of Sharjah in 2016. From 2017 to 2018, he worked as a contracts and estimation engineer.

In January 2019, he joined the Mechanical Engineering master's program in the American University of Sharjah as a graduate teaching and research assistant. His research interests are in experimental and computational solid and fluid mechanics.